Function and Mechanism Study of Light-driven Ion Pumps from Marine Bacteria

海洋性細菌由来の光駆動イオンポンプに対する機能およびメカニズムの研究

2015

Yoshitaka Kato

Department of Frontier Materials

Nagoya Institute of Technology

CONTENTS

Chapter 1

Introduction and Background

Microbial rhodopsin

Microbial rhodopsin is a family of photoreceptor protein which binds retinal and has seven transmembrane helix.[1] The first microbial rhodopsin, bacteriorhodopsin (BR) discovered from a halophilic archaea, *Halobacterium salinarum* in 1971.[3,4] BR was expressed only under oligotrophic condition, and generate the H^+ gradient across the cell membrane from sun light. This H^+ gradient can be used for producing ATP via ATP synthase.[5,6] BR has been recognized as a part of emergency energy producing system of extremophile for a long time. After the discovery of BR, light driven chloride (Cl^-) pump, halorhodopsin (HR) was found from *Halobacterium salinarum* in 1977.[5,6] Two other proeins which act as sensor (sensory rhodopsin I and II) were also found from same bacteria.[7,8,9] Until early 1990s, the homologous proteins were found from other halophilic archea. Although the amino acid sequence of these proteins are different from BR and HR identified from *H. salinarum*, the proteins remain proton pump or chloride pump function. In the case of archaerhodopsin-1 (AR1), the amino acid identity with BR is 59 %. In these days, it was recognized that microbial rhodopsins are specific for extremophile such as halophilic archaea. And, these protein family was called archaeal rhodopsin. Since about 2000, BR-like genes were found from many kind of organism such as cyanobacteria, proteobacteria, fungus and algae. Especially, it is large event for microbial rhodopsin study that Metagenomic analysis reveal many marine bacteria have BR-like gene. [10] Proteins encoded in these gene are generally called proeorhodopsin (PR).[10] PR takes proton (H^+) up from cytoplasmic side to extracellular side same as BR. This discovery indicate the possibility that microbial rhodopsins contribute to large amount of carbon circulation because ocean is 70 % occupancy of the earth surface.[11]

Ion-transport rhodopsin

Microbial rhodopsins have diversity of function, ion-transport, signal transduction, gene regulation and enzymic reaction. Ion-transport rhodopsin is most famous function and is studied well. Actually, bacteriorhodopsin is recognaized as most studied H^+ pump. Recently, ion-transport rhodopsins are used for neural excitation and silencing. Green fluorescent protein (GFP) which is found from *Aequorea Victoria* in 1960's allow us visualize cellar tissue. This visualizing method is widely used from 1990's. Nowadays, we can not only visualize but also control cell and animal behave by using light-driven ion-transport rhodopsins. This control methods is rapidly spread throughout neuroscience field from 2005. The technique using these methods is called "Optogenetics". Most famous optogenetic tool is channel rhodopsin (ChR) which was first discovered from green algae. ChRs function as light-gated cation (proton) channel and can excite neuron by transport cation across lipid bylayer only when it receive photon. Archerhodopsin3 (AR3, light-gated H^+ pump) and HR (light-gated Cl^- pump) were used for silencing neuron.

In 2013-2014, new types of rhodopsin were found from marine bacterium. First one is light-driven sodium pump rhodopsin (NaR). NaR hold the potential to be used as efficient neural silencing tool. Second one is light-driven Cl^- pump rhodopsin (ClR) which have different sequence motif from HR. Although the function of ClR is not new, but comparison between HR and ClR family should allow us understand Cl^- pumping mechanism more. In this thesis, I focused these two rhodopsins to reveal these functional mechanisms.

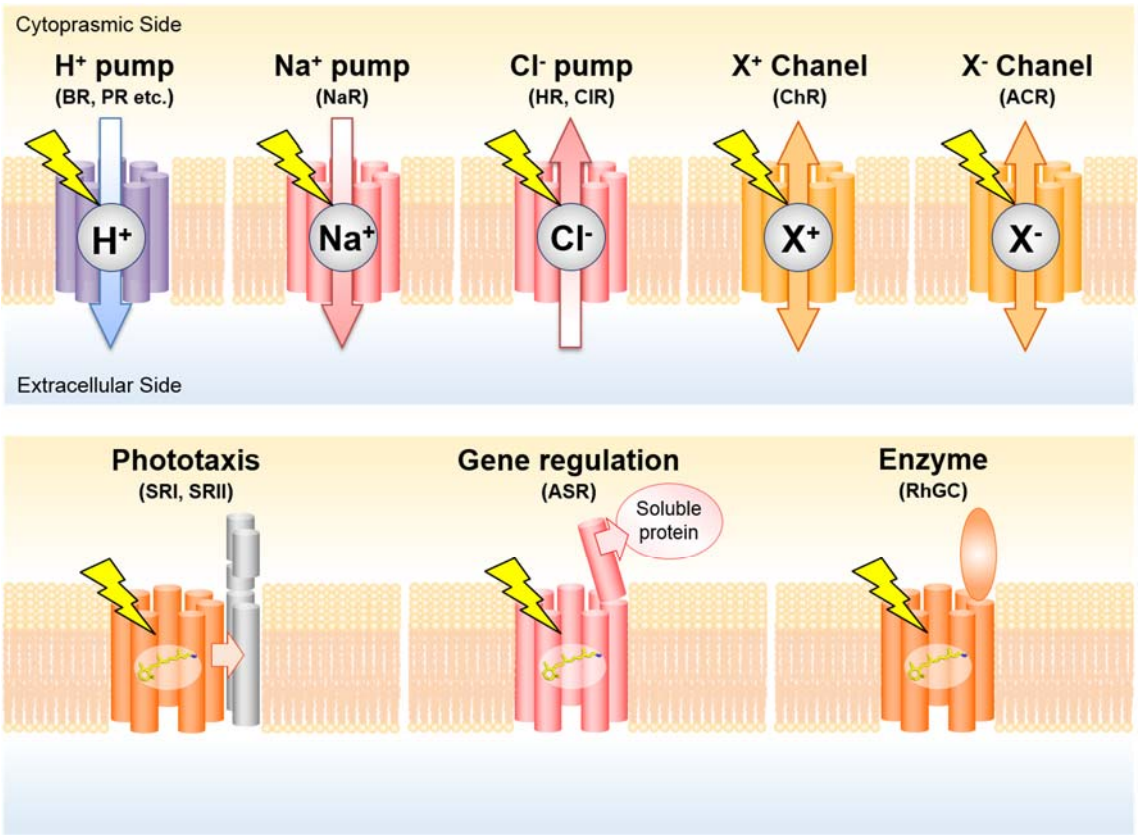

Figure. 1-1 Diversity of function in microbial rhodopsin family proteins.

(Top) Microbial rhodopsins which transport ion were shown. (Bottom) Microbial rhodopsins which have sensor or enzymatic functions were shown.

Structure & photorecation of microbial rhodopsin

Microbial rhodopsin has hepta-helical transmembrane domain, and conject retinal to its lysine residue of 7th helix (G-helix).[1] The retinal binding site is constructed by some amino acid of seven helices. These features are similar to animal rhodopsin which is well-known as visual sensor. After photo-reception, retinal is isomerized from all-*trans* form to 13-*cis* form. The retinal isomerization induce the structural change of protein backbone surrounding retinal. And then, some quasi-stable intermediate states were formed. Finally, these intermediate states thermodynamically decay and get back to initial state. This sequential cyclic reaction was called “photocycle”. The functions were exerted during the photocycle.

M intermediate is one of important intermediate which have deprotonated Schiff base. In the case of BR, Schiff base proton was transferred to counter ion, Asp85. This event induce large blue-shift on its spectra, and is called “M intermediate”. M is formed in most of H^+ pump rhodopsins, but not in Cl^- pump. The spectral changes in photocycle are used for guess functional mechanism of the rhodopsin.

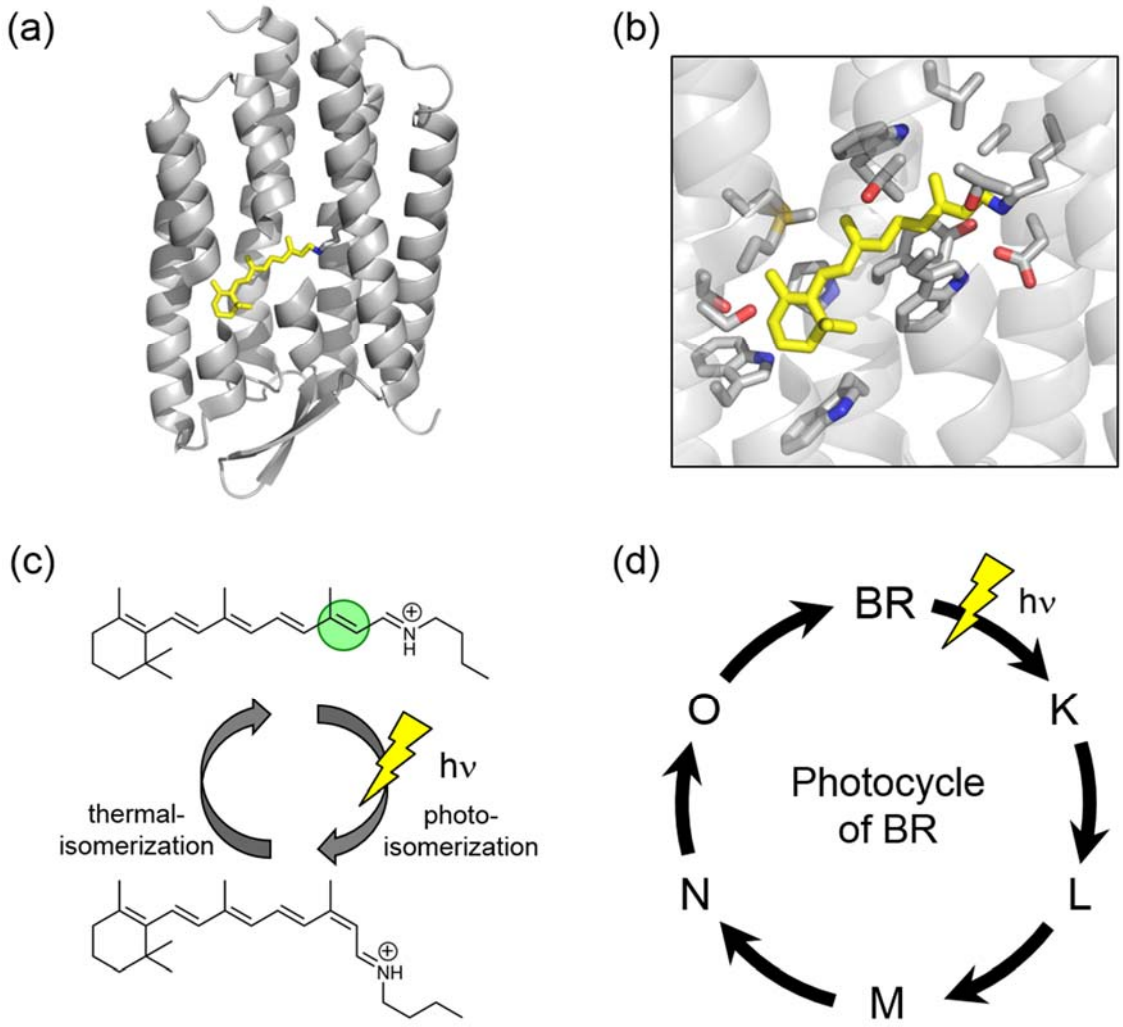

Figure. 1-2 Structure and photoreaction of bacteriorhodopsin

(a) Crystal structure of BR (PDB ID: 1C3W). (b) Retinal binding site was enlarged. Retinal and amino acids surrounding retinal were shown by stick model. (c) The primary reaction of photocycle is isomerization of all-*trans* retinal. 13-cis retinal is eventually converted to all-*trans* retinal. (d) Photocycle of BR. Quasi-stable photo-intermediate states were shown.

Reference

1 Ernst, O.P. et al. (2014) Microbial and animal rhodopsins: structures, functions, and molecular mechanisms. *Chem. Rev. 114,* 126–163

2 Spudich, J.L. and Jung, K-H. (2005) Microbial rhodopsin: phylogenetic and functional diversity. In Handbook of Photosensory Receptors, (Briggs, W.R. and Spudich, J.L., eds), pp. 1–23, *Wiley-VCH Verlag GmbH & Co*

3 Oesterhelt, D. and Stoeckenius, W. (1971) Rhodopsin-like protein from the purple membrane of Halobacterium halobium. *Nat. New Biol.* 233, 149–152

4 Grote, M. (2013) Purple matter, membranes and 'molecular pumps' in rhodopsin research (1960s-1980s). *J. Hist. Biol. 46*, 331–368

5 Matsuno-Yagi, A. and Mukohata, Y. (1977) Two possible roles of bacteriorhodopsin; a comparative study of strains of Halobacterium halobium differing in pigmentation. *Biochem. Biophys. Res. Commun. 78*, 237–243

6 Schobert, B. and Lanyi, J.K. (1982) Halorhodopsin is a light-driven chloride pump. *J. Biol. Chem. 257*, 10306–10313

7 Bogomolni, R.A. and Spudich, J.L. (1982) Identification of a third rhodopsin-like pigment in phototactic Halobacterium halobium. *Proc. Natl. Acad. Sci. U.S.A. 79*, 6250–6254

8 Takahashi, T. et al. (1985) A photosystem other than PS370 also mediates the negative phototaxis of Halobacterium halobium. *FEMS Microbiol. Lett. 28*, 161–164

9 Inoue, K. et al. (2013) Molecular and evolutionary aspects of microbial sensory rhodopsins. *Biochim. Biophys. Acta 1837*, 562–577

10 Béjá , O. et al. (2000) Bacterial rhodopsin: evidence for a new type of phototrophy in the sea. *Science 289*, 1902–1906

11 Yoshizawa, S. et al. (2012) Diversity and functional analysis of proteorhodopsin in marine flavobacteria. *Environ. Microbiol. 14*, 1240–1248

Chapter 2

Structural basis for Na^+ transport mechanism by a light-driven Na^+ pump

2-1 Introduction s

Microbial rhodopsin is a well-studied protein family which widely distributed in microorganisms.[1] First microbial rhodopsin, bacteriorhodopsin (BR) was identified from membrane of a Halophilic archaea, *Halobacterium salinarum* in 1971.[2] Its function is identified as light-driven proton pump.[3] BR was expressed only under oligotrophic condition, and generate the H^+ gradient across the cell membrane from sun light. This H^+ gradient can be used for producing ATP via ATP synthase.[4,5] BR had been recognized as a part of emergency energy producing system of extremophile for a long time. After the discovery of BR, light-driven chloride pump, halorhodopsin (HR)[6,7] and two phototaxis sensor, sensory rhodopsins (SRI and SRII)[8-10] were identified from *H. salinarum*. Although some homologous proteins were discovered until early 1990s, their functional varieties and the microorganisms containing the homologous proteins were limited.[11-15] Since 2000, two important events occur. One is the discovery of channelrhodopsins from green algae, *Chlamydomonas reinhardtii*.[16-18] These proteins has fundamental structural feature such as heptahelical transmembrane domain and the conjugation of retinal Schiff base seen in haloarchaeal microbial rhodopsins, but their amino acid sequences are largely different from the haloarchaeal types. ChR can transport cation along with the electrochemical gradient. Whereas light-gated ion pump transports only one ion during the photoreaction triggered by one photon, light-gated ion channel, ChR transport a lot of ion the photoreaction triggered by one photon. Because of this difference, the current produced by ChR is higher than light-driven ion pumps. After the discovery, ChR was used for neuro and brain science. Contrary with visualizing method using green fluorescent protein, ChR can stimulate neuron and control animal behaver.[19-21] This

strong technique was rapidly spread along with the word "optogenetics" in biology field.[22] Another important event was metagenomic analysis of marine bacterium.[23,24] The genomic analysis shows that microbial rhodopsins are widely distributed among marine bacteria living the ocean which occupy 70 % of the earth surface.[25] These studies and the H^+ transport assays on native cell[26] indicate that microbial rhodopsin is not minor protein family and take significant contribution to the carbon circulation. From amino acid sequence, most of rhodopsins found from marine bacteria were thought to be light-driven proton pumps. But, in 2013, new rhodopsin which pumps Na^+ is discovered from a marine bacteria, *Krokinobacter eikastus* (KR2).[27] In general, microbial rhodopsin has seven transmembrane helices, but three of these (helix D, E and F) may not directory constitute ion transport pathway because these domain should hold hydrophobic domain of retinal chromophore (β-ionone ring and polyene chain). Thus, the ion transport pathway should be constructed by remaining helices. Furthermore, one of the remaining helices, helix G conjugate retinal by forming protonated (positively charged) Schiff base. Although, the Schiff base can be transiently deprotonated by transferring H^+ to acceptor during photocycle, it was historically thought that rhodopsin cannot pump cation except H^+. In the case of H^+ pump, it is possible to construct H^+ transport pathway because Schiff base can be included H^+ transport pathway.[1] Although ChR can transport cation, its transport is not unidirectional and against electrochemical gradient.[18,] How does Na^+ pump rhodopsin resolve described structural limitation? Thus, the structural information of Schiff base region is needed for understanding Na^+ pump mechanism of KR2. The newly obtained X-ray crystallographic structure of KR2 showed that specific structural features. Here, we examine the responsibilities of some amino acids constructing the features.

2-2 Materials & Methods

Protein Expression, and Purification

For biochemical and spectroscopic experiments (ion transport activity assay, flash photolysis, quantification of KR2 expression in *E. coli*), we mainly used a synthesized KR2 gene whose codons were optimized for *E. coli* expression[28]. The KR2 gene was **inserted into pET-vector with C-terminal 6x His-tag.** The protein was expressed in C41 (DE3) *E. coli* cells, induced with 1 mM isopropyl β-D-thiogalactopyranoside (IPTG) and supplemented with 10 μM all-trans-retinal (Sigma) for 3 hours at 37°C. The cells were disrupted and the membrane fraction was collected by ultracentrifugation (35,000 rpm, 60 min). The corrected membrane fraction including KR2 was solubilized with 2% n-dodecyl- β-D-maltoside (DDM) in buffer (50 mM HEPES, 300 mM NaCl, pH 7.0). The solubilized KR2 was purified using Co-NTA affinity column (TALON, Quiagen) chromatography. The KR2 was finally eluted using the buffer including 300 mM Imidazole (50 mM Tris-HCl, 300 mM NaCl, 300 mM Imidazole, and 0.1 % DDM at pH 7.0). The purified KR2 in DDM was mixed with 1,2-Dioleoyl-sn-glycero-3-phosphocholine, DOPC (molar ratio of KR2:DOPC = 1:20) and reconstituted into DOPC. DDM was removed by Bio-beads SM-2 (Bio-Rad, Hercules, CA).

Ion transport activity assay

E. coli expressing KR2 were cultured as described previously[27]. The *E. coli* were collected by centrifugation (7000 rpm, 3 min), washed three times with 100 mM NaCl, and re-suspended in the same solution. For K^+ pump assay, the cells were washed and suspended in 100 mM KCl in a similar manner. The *E. coli* suspension (7.5 mL) was putted into a temperature-controlled measurement cell in darkness. And then, pH of the suspension was measured by pH meter (F-55, Horiba, Japan). After stabilization of pH, the suspension was

illuminated using 1-kW tungsten–halogen projector lamp (Master HILUX-HR, Rikagaku, Japan) through a glass filter (Y-52, AGC Techno Glass, Japan) for 150 sec. When Na^+ was transported, secondary H^+ movement occur in order to let off charge imbalance. This light-induced pH changes were measured by pH meter. The measurements were repeated under the same conditions after the addition of 10 μM CCCP.

Flash photolysis

The transient absorption spectra of KR2 mutants were measured by a flash photolysis system, using a multichannel detector (Hamamatsu Photonics, Japan). KR2 reconstituted into DOPC was suspended in buffer (50 mM Tris–HCl, 100 mM NaCl, pH 8.0). The sample suspension was placed in a quartz cuvette (path length: 10 mm) and excited with a beam of the second harmonics of a nanosecond-pulsed Nd^{3+}-YAG laser (λ = 532 nm, INDI40, Spectra-Physics). The laser power was adjusted to 300 mJ/pulse, and the repetition rate was adjusted to 0.5 Hz, which is slower than the photocycle rate of KR2. The transient absorption spectra of KR2 were obtained by calculating the ratio of the transmitted probe light from a Xe arc lamp (L8004, Hamamatsu Photonics, Japan), with and without laser excitation. The transient absorption change at a specific probe wavelength was obtained by combining the data points at different time-delays (t_{delay} = 80 μs-200 ms).

Quantification of KR2 expressed in E. coli

In order to quantitate the expression level, KR2 expressed in *E. coli* is denatured by adding hydroxylamine. The Schiff base conjugation of retinal is cleaved by hydroxylamine attack with light illumination. This reaction is accompanied by spectral change, because cleaved retinal oxime has blue-shifted spectra which λ_{max} is near 360 nm. The expression level of

KR2 can be calculated from obtained difference spectra. For this quantification analysis, *E. coli* expressing KR2 were centrifuged and suspended in buffer (50 mM Tris–HCl, 100 mM NaCl, pH 8.0), to a final volume of 3 mL. Then, 200 μL of 1 mM lysozyme was added. The *E. coli* cells suspended in buffer were disrupted by ultrasonication, and DDM was added to a final concentration of 3 %. The absorption change was measured using UV-vis spectrometer (V-650, Jasco, Japan) with an integrating sphere (ISV-722, Jasco, Japan) for 30-90 minutes, after the addition of hydroxylamine to a final concentration of 500 mM. The suspension was illuminated using a 1-kW tungsten–halogen projector lamp (Master HILUX-HR, Rikagaku, Japan) through a glass filter (Y-52, AGC Techno Glass, Japan). The molecular extinction coefficient of rhodopsin (ε) was calculated by the ratio between the absorbances of rhodopsin and retinal oxime (ε = 33,900 M^{-1} cm^{-1}), and the amount of KR2 expressed in *E. coli* cells was determined by the absorbance of the bleached rhodopsin and the ε value.

2-3 Results

Overall structure of KR2

Crystal structures of KR2 under low pH and neutral pH were determined by collaborators. The crystals were obtained from KR2 truncated the C-terminal five amino acid residues (residues 1-275) by using lipidic cubic phase method. The detail method and analysis is described in ref. 29. Some specific features were seen in the structures of KR2. First one is extracellular side (BC-loop and N-terminal). Second is cytoplasmic side. Third is Schiff base region including Ser70, Asn112, and Asp116. In this study, we focused on these structures and examine the responsibility for function.

BC-loop and N-terminal helix

According to crystal structure, KR2 have antiparallel β-sheet structure in extracellular BC-loop which connect helix B and C. Extracellular BC-loop has 4 carboxylic residues, Glu89, Glu90, Asp98 and Asp102. In previous study, it is revealed that BC-loop forms Na^+ binding site in initial state. Further experiment showed that D102 is important for Na^+ binding in Initial state, but E89, E90 and D98 are not neccesaly.[29] On the other hand, D102N mutant remain Na^+ transport activity (Fig.2-2) in agreement with the previous result of E89Q/E90Q/D98N/D102N quadruple mutant [27]. These results means that Na^+ binding in initial state is not needed for Na^+ transport function.

In N-terminal extracellular region, Helix structure was observed. This feature is not observed in classical type of microbial rhodopsin such as BR, HR and XR. N-terminal helix has a carboxylic residue, Glu11 which direct to Arg243 in helix G. Arg243 also close to Asp160 in helix D. These three amino acid and some water molecule forms hydrogen bond network. In order to examine the roll of these two structural features, we measured ion transport activity of KR2 mutant in *E. coli* cells by using pH-meter (the method is described in chapter 1). The results were shown in Figure 2-2. The N-terminal truncated KR2 mutant ($KR2_{\Delta 1\text{-}18}$), E11A, E116A, and R243A single amino acid mutants were tried. Although $KR2_{\Delta 1\text{-}18}$ was not expressed enough, single mutants were successfully expressed. Because these mutants remain Na^+ pump activity, we concluded that the structural features seen around N-terminal was not responsible for function.

On the other hand, amino acid sequence of N-terminal region and Asp102 in BC-loop are conserved in putative NaR which have NDQ motif. From this aspect, these feature should have some important role. Thus, we further examine the thermal stability of these mutants, and concluded that these structural features are responsible for thermal stability of NaR.[29]

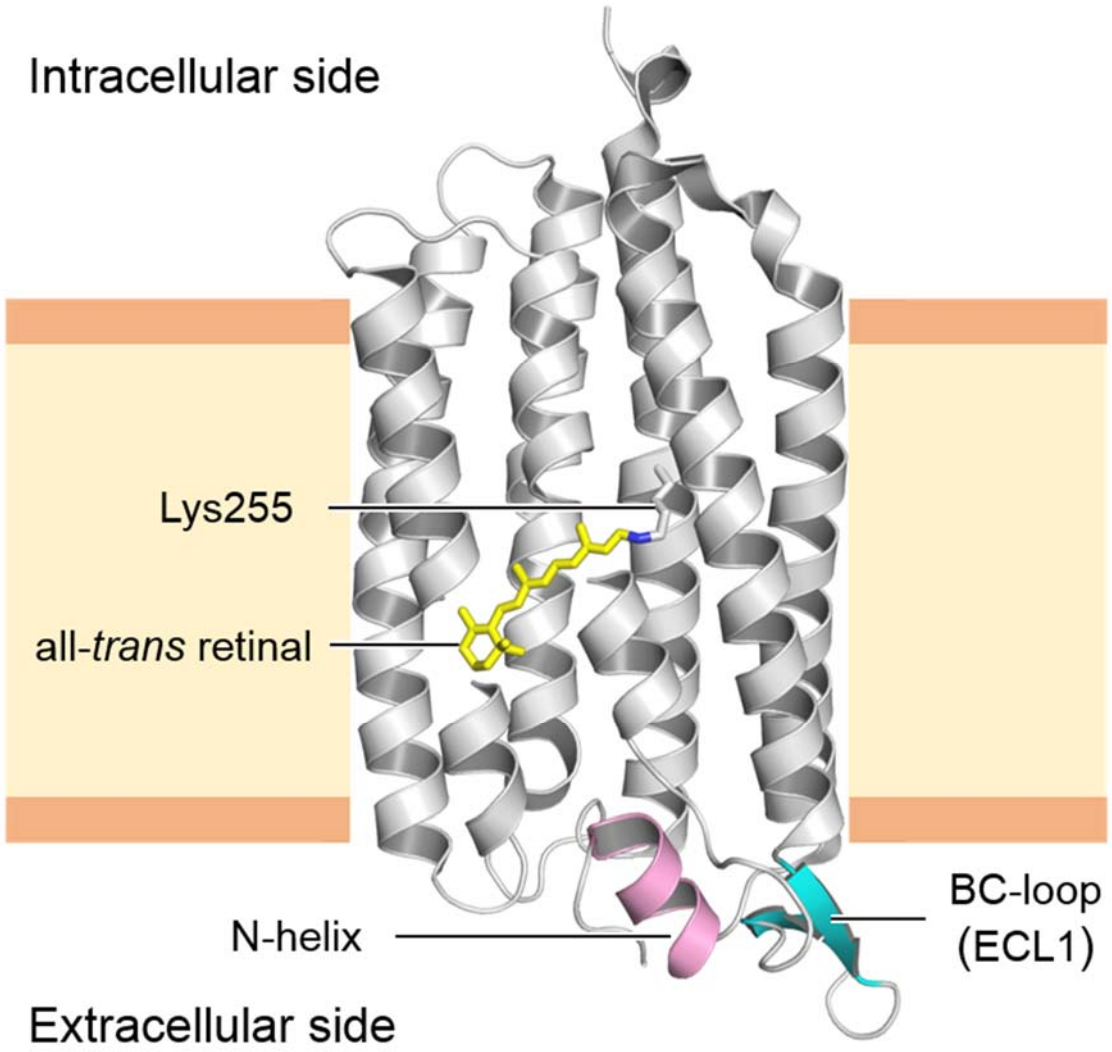

Figure 2-1　Overall structure of KR2

Crystal structure of KR2 (PDB ID: 3X3B), viewed parallel to the membrane. KR2 consists of the N-helix, the seven transmembrane helices, extracellular loops, and intracellular loops. All-trans retinal binding to Lys255 in helix G is shown by stick model. N-terminal helix (pink) and BC loop (cyan) are characteristic structure of KR2 (detail information are described in text).

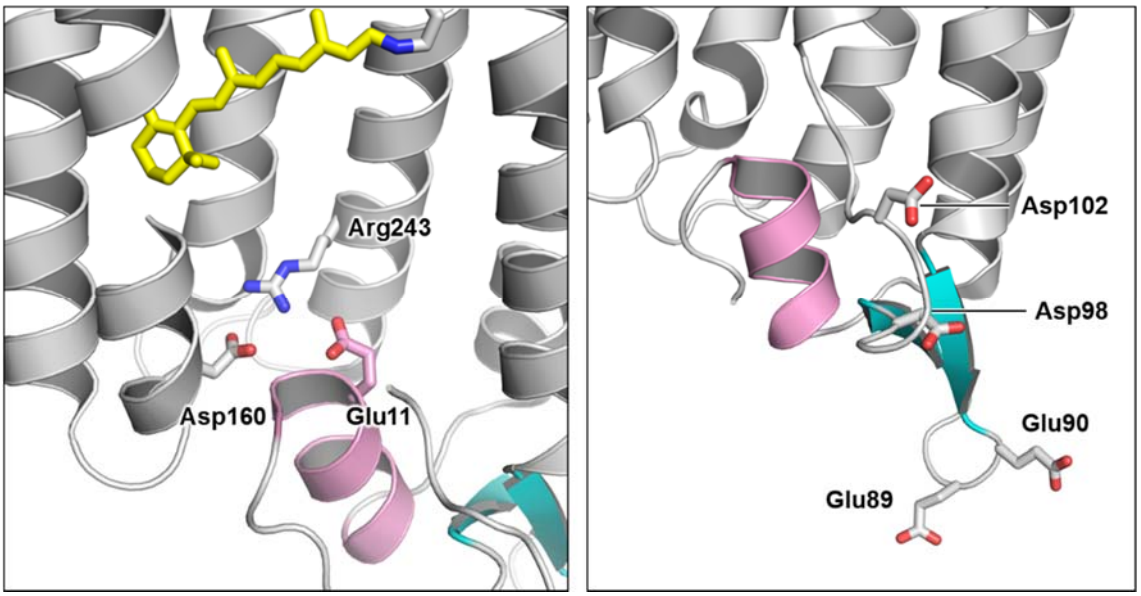

Figure 2-2 Structures of the N-terminal helix and BC-loop.

(Left) N-terminal helix (pink) has a carboxylic residue, Glu11 which direct to Arg243 in helix G. Arg243 also close to Asp160 in helix D. These three amino acid and some water (not shown) forms hydrogen bond network. (Right) BC- loop which has 4 carboxylic residues, Glu89, Glu90, Asp98 and Asp102. (PDB ID: 3X3B)

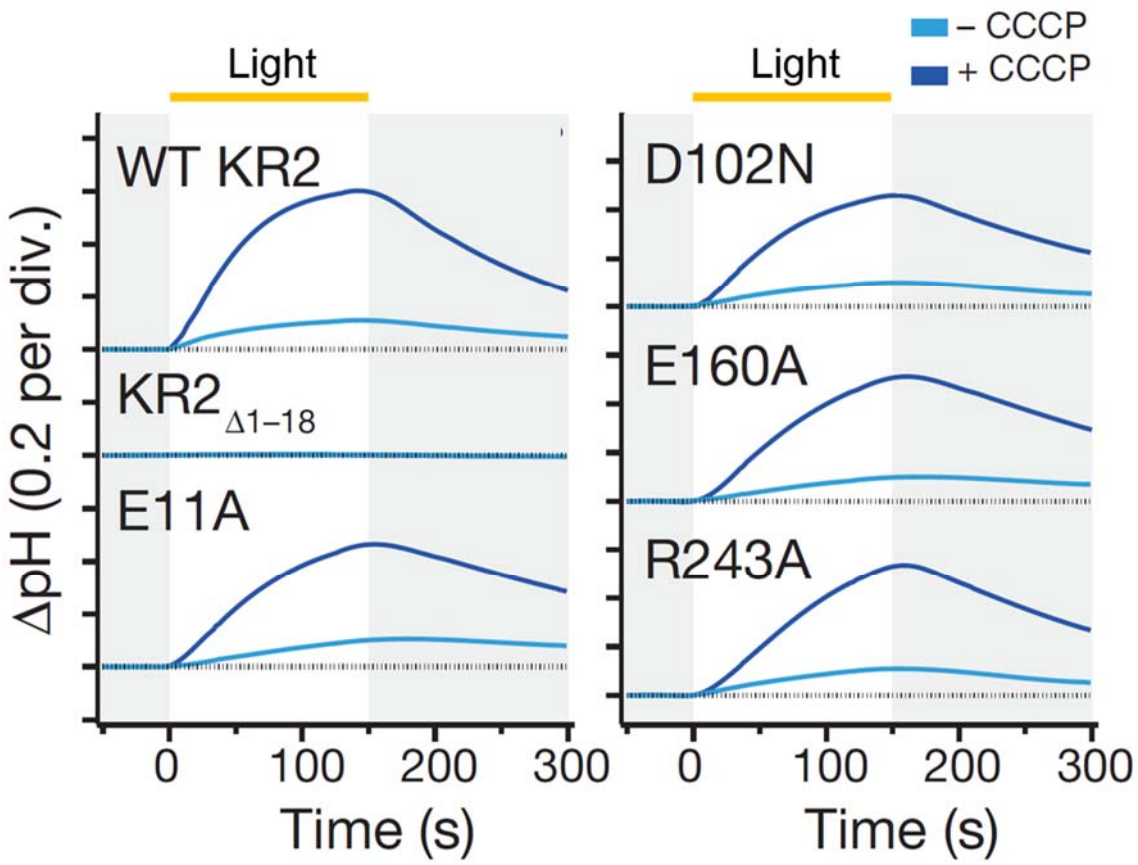

Figure 2-3 Functional analysis of N-terminal and BC-loop mutants

Pump activities of KR2 WT and five mutants in E. coli cell. Cyan and blue trace indicate without and with CCCP, respectively. CCCP is protonophore which enhance H^+ permeability across the lipid cell membrane.

Intracellular cavity

The structural feature of intracellular side which should related to selective Na^+ uptake is one of attractive topics. We next focus the cytoplasmic site. Although the cytoplasmic region is relatively similar to other microbial rhodopsins than the extracellular region, a hydrophilic cavity constituted with Y45, F46 S60, N61, and Q123 was observed. Q123 is highly conserved amino acid for putative NaR and is included NDQ motif. In previous study, Na^+ transport activity of Q123X mutants were already measured. These mutants have week Na^+ transport activity. Here, we tried to examine the dynamics of photoreaction. In previous study, we concluded that Na^+ uptake occurs during formation of O intermediate (which couple with decay of L/M intermediate). In the photocycle of KR2 Q123A, the kinetics of L/M and O decay becomes slow. The L/M decay kinetics of Q123A mutant ($\tau_{L/M}$ = 5.5 ms) is more than five times slower than that of WT ($\tau_{L/M}$ = 1.0 ms). The O decay kinetics of Q123A mutant (τ_O = 22 ms) is more than three times slower than that of WT (τ_O = 7.9 ms). The result of photocycle and X-ray structure indicate that Q123 contribute to Na^+ uptake. The position of Q123 in KR2 corresponds to that of D96 in BR. In the case of BR, D96 is one of important residues for H^+ pump function and is called internal proton donor of Schiff base. During the photocycl of BR, Schiff base is deprotonated (M intermediate). The deprotonated Schiff base receive H^+ from D96 during M decay transition. D96 mutation (X = N, A and G) slow down M decay (WT: τ_M ≈ 7 ms, D96N: τ_M ≈ 200 ms at pH 7) and decrease H^+ pump activity because H^+ uptake becomes less efficient than WT. Most of discovered H^+ pump rhodopsin have carboxylic acid in this position. As compared with the effect of D96 mutation in BR, Q123 mutation in KR2 is not effective for photocycle. This may be attributed to differences of structure and mechanism between BR and KR2. In the case of KR2, the possible Na^+ uptake site is constituted by some amino acids. Furthermore M intermediate seems to be at equilibrium with L.

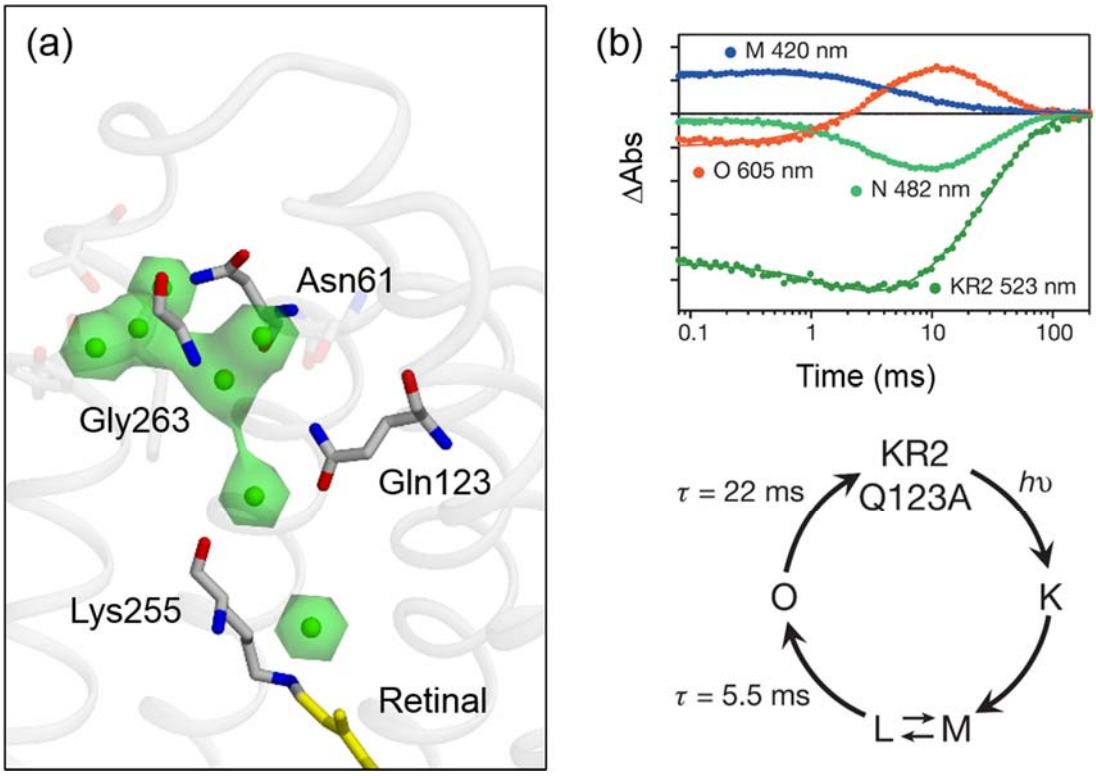

Figure 2-4　The intracellular hydrophilic cavity of KR2

(a) The Internal hydrophilic cavity are constructed by Tyr45, Phe46, Thr49, Ser60, Asn61, Gln123 and Gly253. In this study, Asn61, Q123, and Gly263 were mutated. Water molecules are shown by green sphere and surface (PDB ID: 3X3B). (b) The photoreaction of KR2 Q123A mutant.

Schiff base region

The Crystal structures of KR2 at acidic pH (pH 4.0) and neutral pH (pH 7.0) were obtained by collaboration study. The differences are observed near Schiff base region between these two structures. We measured the spectral properties of WT, D116N, and D253N. In the case of WT, the absorption maxima (λ_{max}) at pH 7.0 was red-shifted for ca. 10 nm (pH 7.0: 526 nm, pH 4.0: 536 nm). λ_{max} of D253N mutant was close to WT.[29] On the other hands, λ_{max} of D116N mutant was red-shifted from that of WT at pH 7.0 (D116N: 558 nm at pH 7.0) indicating that pH dependent λ_{max} shift is related to protonation state of D116. The photoreaction of D116N mutant was similar to that of WT at acidic pH. Thus, it is suggested that D116 of KR2 is deprotonated and act as counter ion of protonated Schiff base. According to crystal structures, the formation of the hydrogen bond network among S70, N112 and D116 seems to prevent the structural limitation and open up Na^+ transport pathway. In order to examine this hypothesis, we try to measure ion transport activity of KR2 S70A and N112A mutants. The side chain (methyl group) of the alanine introduced to position at S70 and N112 cannot form hydrogen bond with carboxylate group of D116. These mutation decrease Na^+ transport activity. These results may attributed to loss of hydrogen bond. Thus, we concluded that the hydrogen network among S70, N112 and D116 is responsible for opening up Na^+ transport pathway. From these experiments, the mechanism of H^+ pump function of KR2 in absence of Na^+ cannot be discussed well.

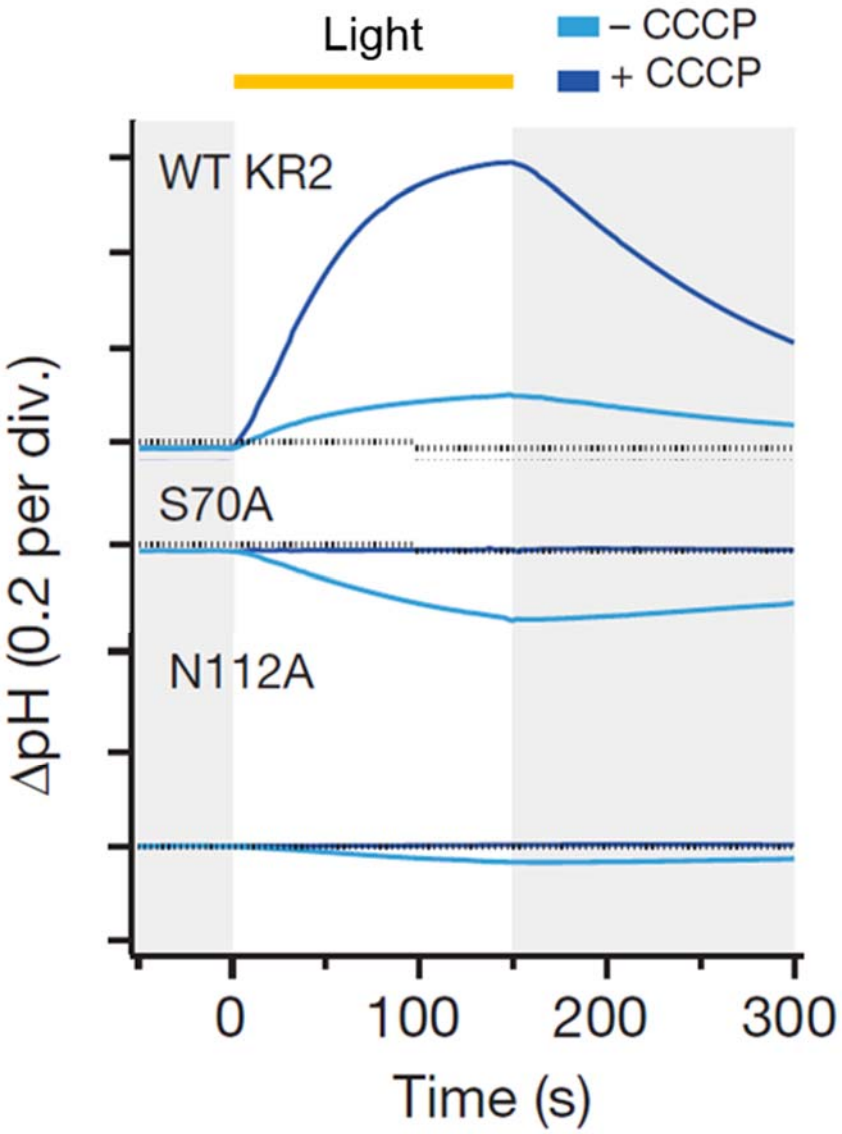

Figure 2-5 Functional analysis of S70A and N112A mutants

Pump activities of KR2 WT and two mutants in E. coli cell. Cyan and blue trace indicate without and with CCCP, respectively. CCCP is protonophore which enhance H^+ permeability across the lipid cell membrane.

KR2 application to optogenetics

Outward cation pump have a potential for neural silencing tool similar with inward chloride pump and outward proton pump. Because Na^+ concentration is ten times lower than Na^+ concentration in mammalian cell, outward potassium pump is more useful than sodium pump. But, wild type KR2 cannot pump K^+. Thus, we try to create engineered cation pump which can transport K^+ by introducing site-specific mutation to KR2. As described before, several amino acids constituting cytoplasmic cavity were identified. These amino acids should related to cation selectivity and are candidate of mutation site. The effective mutation sites are the positions of N61 and G263 (Figure 2-4). We revealed that KR2 N61P/G263W mutant can transport K^+ (Figure2-6). The signal in presence of KCl is larger than that in presence of NaCl. These results indicate that K^+ selectivity becomes higher than Na^+ selectivity in this mutant.

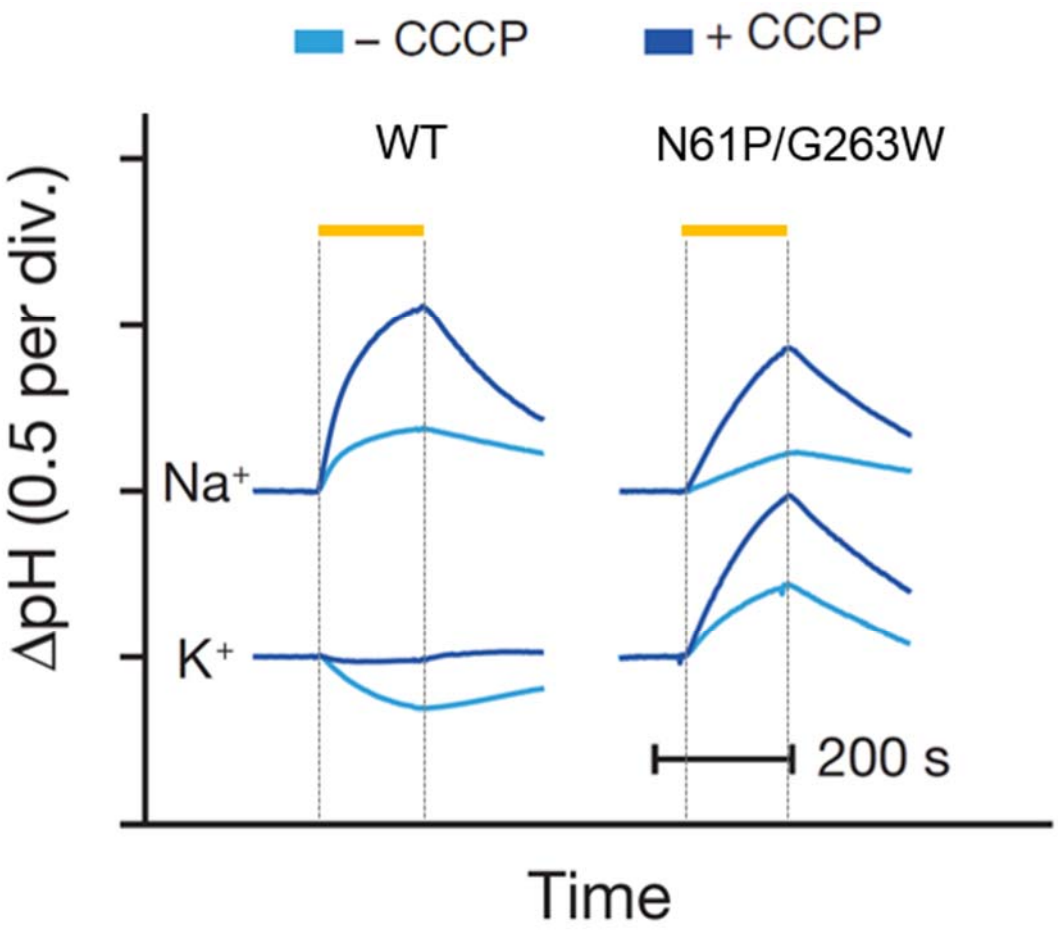

Figure 2-6 Engineering of light-driven potassium pump

Pump activities of KR2 WT and N61P/G263W mutant in *E. coli* cell were measured in 100 mM NaCl (top) or 100 mM KCl (bottom). Cyan and blue trace indicate without and with CCCP, respectively. CCCP is protonophore which enhance H^+ permeability across the lipid cell membrane.

2-4 Discussion

We suggest a model of Na^+ transport mechanism based on the results about Schiff base region (Figure 2-7). In initial state, KR2 has positively-charged protonated Schiff base which blocks cation accessing. After light reception, all-*trans* retinal was isomerized to 13-*cis* form, and K intermediate was formed. In previous FTIR study, we showed that K intermediate cannot distinguish between Na^+ and H^+. When M intermediate was formed, Schiff base donate H^+ to carboxylic acid of D116. Present study indicate that this proton transfer induce the rotation of D116 residue, and that the hydrogen bond network among S70, N112 and D116 is formed. This local structural change takes a role as gating of Na^+ transport pathway near Schiff base. After Na^+ uptake, the collapse of the hydrogen bond network among S70, N112 and D116, and back H^+ transfer from D116 to Schiff base may occur. This state should be attributed to O intermediate identified by previous flash photolysis measurement. We reanalyzed the absolute absorption spectra of O intermediate from previous flash photolysis data in NaCl and LiCl.[27] The spectra in NaCl was red-shifted from that in LiCl indicating that O intermediate bind cation near retinal chromophore. This spectral shift should support present transport model.

We also achieved to create light-driven potassium pump based on the crystal structure. The mutation of two amino acids (N61 and G263) near internal hydrophilic cavity change cation selectivity of KR2. Although these two amino acids are related to cation selectivity, we cannot conclude how the mutation modify the selectivity in this study. The cation selective mechanism is one of important topics for cation transport protein. In chapter 4, we will show further experiments of the mutants, and suggest a model of the mutation effect.

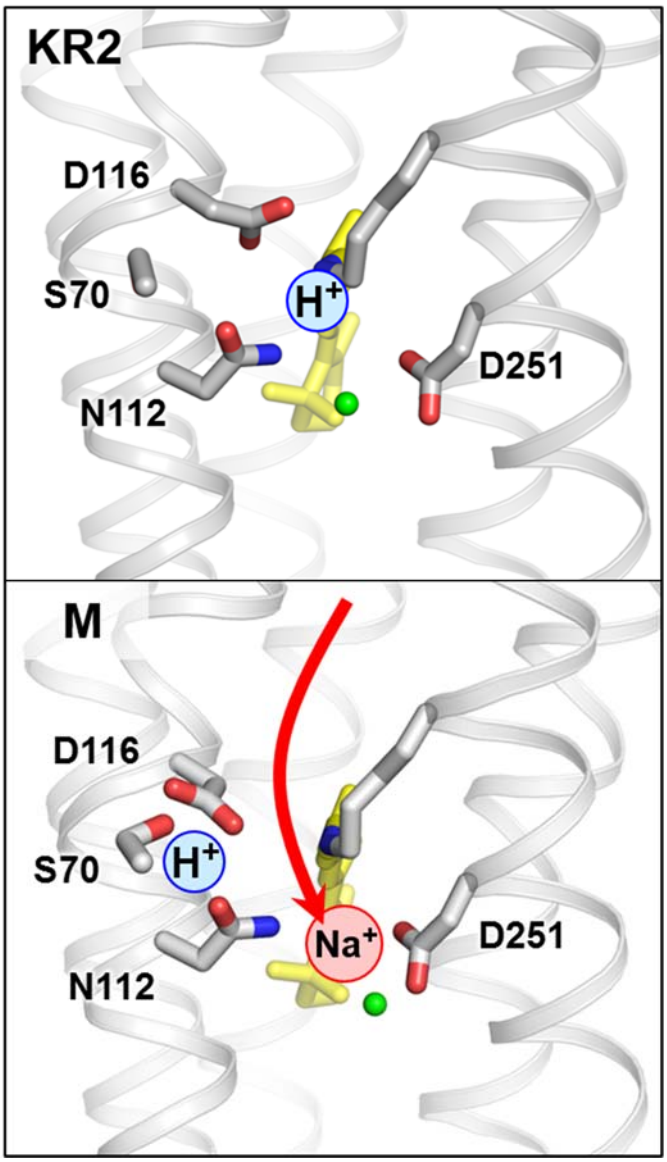

Figure 2-7　Model of Na^+ transport.

(Top, PDB ID: 3X3C) In the dark state, Schiff base is protonated and positively-charged. (Bottom PDB ID: 3X3B) In the M intermediate, proton is already transferred from Schiff base to D116. Side chain of protonated D116 rotate and forms hydrogen bonds with S70 and N112. This local structural change allow　Na^+ uptake.

Reference

1 Ernst, O. P.; Lodowski, D. T.; Elstner, M.; Hegemann, P.; Brown, L. S.; Kandori H. Microbial and Animal Rhodopsins: Structures, Functions, and Molecular Mechanisms. *Chem. Rev.* 2014, *114*, 126-63.

2 Oesterhelt, D.; Stoeckenius, W. Rhodopsin-Like Protein from the Purple Membrane of *Halobacterium Halobium*. *Nat. New Biol.* 1971, *233*, 149-152.

3 Oesterhelt, D.; Stoeckenius, W. Functions of a new photoreceptor membrane. *Proc. Natl. Acad. Sci. USA.* 1973, *70*, 2853-7.

4 Racker, E.; Stoeckenius, W. Reconstitution of Purple Membrane Vesicles Catalyzing Light-driven Proton Uptake and Adenosine Triphosphate Formation. *J Biol Chem.* 1974, *249*, 662-3.

5 Hartmann, R.; Sickinger, H. D.; Oesterhelt, D. Quantitative aspects of energy conversion in halobacteria. *FEBS Lett.* 1977, *82*, 1-6.

6 Matsuno-Yagi, A.; Mukohata, Y. Two possible roles of bacteriorhodopsin; a comparative study of strains of Halobacterium halobium differing in pigmentation. *Biochem. Biophys. Res. Commun.* 1977, *78*, 237-43.

7 Schobert, B.; Lanyi, J. K. Halorhodopsin is a Light-Driven Chloride Pump. *J. Biol. Chem.*1982, *257*, 10306-13.

8 Bogomolni, R. A.; Spudich, J. L. Identification of a Third Rhodopsin-like Pigment in Phototactic *Halobacterium Halobium*. *Proc. Natl. Acad. Sci. USA.* 1982, *79*, 6250-4.

9 Takahashi, T.; Tomioka, H.; Kamo, N.; Kobatake, Y. A Photosystem Other than PS370 also Mediates the Negative Phototaxis of *Halobacterium Halobium*, *FEMS Microbiol. Lett*. 1985, *28*, 161–164

10 Inoue, K.; Tsukamoto, T.; Sudo, Y. Molecular and Evolutionary Aspects of Microbial Sensory Rhodopsins. *Biochim Biophys Acta.* 2014, *1837*, 562-77.

11 Bivin, D. B..; Stoeckenius, W. Photoactive Retinal Pigments in Haloalkaliphilic Bacteria. *J. Gen. Microbiol.* 1986, *132*, 2167-77.

12 Mukohata Y, Sugiyama Y, Ihara K, Yoshida M. An Australian Halobacterium Contains a Novel Proton Pump Retinal Protein: Archaerhodopsin. *Biochem. Biophys. Res. Commun.* 1988, *151*, 1339-45.

13 Uegaki, K.; Sugiyama, Y.; Mukohata, Y.; Archaerhodopsin-2, from Halobacterium sp. aus-2 Further Reveals Essential Amino Acid Residues for Light-driven Proton Pumps. *Arch. Biochem. Biophys.* 1991, *286*, 107-10.

14 Otomo, J.; Tomioka, H.; Sasabe, H. Bacterial Rhodopsins of Newly Isolated Halobacteria. *J. Gen. Microbiol.* 1992, *138*, 2389-96.

15 Sugiyama, Y.; Yamada, N.; Mukohata, Y. The Light-driven Proton Pump, Cruxrhodopsin-2 in Haloarcula sp. arg-2 (bR+, hR-), and its coupled ATP formation. *Biochim Biophys Acta.* 1994, *1188*, 287-92.

16 Nagel, G.; Ollig, D.; Fuhrmann, M.; Kateriya, S.; Musti, A. M.; Bamberg, E.; Hegemann, P. Channelrhodopsin-1: a Light-gated Proton Channel in Green Algae. *Science* 2002, *296*, 2395-8.

17 Nagel, G.; Szellas, T.; Huhn, W.; Kateriya, S.; Adeishvili, N.; Berthold, P.; Ollig, D.; Hegemann, P.; Bamberg, E. Channelrhodopsin-2, a Directly Light-Gated Cation-Selective Membrane Channel. *Proc. Natl. Acad. Sci. USA* 2003, *100*, 13940−13945.

18 Sineshchekov, O. A.; Govorunova, E. G.; Dér, A.; Keszthelyi, L. Nultsch, W. Photoinduced Electric Currents in Carotenoid-Deficient Chlamydomonas Mutants Reconstituted with Retinal and Its Analogs. *Biophys J.* 1994, *66*, 2073-84.

19 Boyden, E. S.; Zhang, F.; Bamberg, E.; Nagel, G.; Deisseroth, K. Millisecond-Timescale, Genetically Targeted Optical Ccontrol of Neural Activity. *Nat. Neurosci.* 2005, *8*, 1263-8.

20 Li, X.; Gutierrez, D. V.; Hanson, M. G.; Han, J.; Mark, M. D.; Chiel, H.; Hegemann, P.; Landmesser, L. T.; Herlitze, S. Fast Noninvasive Activation and Inhibition of Neural and Network Activity by Vertebrate Rhodopsin and Green Algae Channelrhodopsin. *Proc. Natl. Acad. Sci. USA* 2005, *102*, 17816-21.

21 Witten, I.B.; Lin, S. C.; Brodsky, M.; Prakash, R.; Diester, I.; Anikeeva, P.; Gradinaru, V.; Ramakrishnan, C.; Deisseroth, K. Cholinergic Interneurons Control Local Circuit Activity & Cocaine Conditioning. *Science* 2010, *330*, 1677-81.

22 Adamantidis, A.; Arber, S.; Bains, J. S.; Bamberg, E.; Bonci, A.; Buzsáki, G.; Cardin, J. A.; Costa, R. M.; Dan, Y.; Goda, Y.; Graybiel, A. M.; Häusser, M.; Hegemann, P.; Huguenard, J. R.; Insel, T. R.; Janak, P. H.; Johnston, D.; Josselyn, S. A.; Koch, C.; Kreitzer, A. C.; Lüscher, C.; Malenka, R. C.; Miesenböck, G.; Nagel, G.; Roska, B.; Schnitzer, M. J.; Shenoy, K. V.; Soltesz, I.; Sternson, S. M.; Tsien, R. W.; Tsien, R. Y.; Turrigiano, G. G.; Tye, K. M.; Wilson, R. I. Optogenetics: 10 Years after ChR2 in Neurons—Views from the Community. *Nat. Neurosci.* 2015, *18*, 1202-12.

23 Béjà, O.; Aravind, L.; Koonin, E. V.; Suzuki, M. T.; Hadd, A.; Nguyen, L. P.; Jovanovich, S. B.; Gates, C. M.; Feldman, R. A.; Spudich, J. L.; Spudich, E. N.; DeLong, E. F.

Bacterial Rhodopsin: Evidence for a New Type of Phototrophy in the Sea. *Science* 2000, *289*, 1902-6.

24 Béjà, O.; Spudich, E. N.; Spudich, J. L.; Leclerc, M.; DeLong, E. F. Proteorhodopsin Phototrophy in the Ocean. *Nature* 2001, *411*, 786-9.

25 Fuhrman, J. A.; Schwalbach, M. S.; Stingl, U. Proteorhodopsins: an Array of Physiological Roles? Nat. Rev. Microbiol. 2008, *6*, 488-94.

26 Yoshizawa, S.; Kawanabe, A.; Ito, H.; Kandori, H.; Kogure, K. Diversity and Functional Analysis of Proteorhodopsin in Marine Flavobacteria. *Environ. Microbiol.* 2012, *14*, 1240-8

27 Inoue, K.; Ono, H.; Abe-Yoshizumi, R.; Yoshizawa, S.; Ito, H.; Kogure, K.; Kandori, H. A Light-driven Sodium Ion Pump in Marine Bacteria. *Nat. Commun.* 2013, *4*, 1678.

28 Ono, H.; Inoue, K.; Abe-Yoshizumi, R.; Kandori, H. FTIR Spectroscopy of a Light-driven Compatible Sodiumion-Proton Pumping Rhodopsin at 77K. *J. Phys. Chem. B* 2014, 118, 4784–4792.

29 Kato, H. E.; Inoue, K.; Abe-Yoshizumi, R.; Kato, Y.;, Ono, H.; Konno, M.; Hososhima, S.; Ishizuka, T.; Hoque, M. R.; Kunitomo, H.; Ito, J.; Yoshizawa, S.; Yamashita, K.; Takemoto, M.; Nishizawa, T.; Taniguchi, R.; Kogure, K.; Maturana, A. D.; Iino, Y.; Yawo, H.; Ishitani, R.; Kandori, H.; Nureki, O. Structural basis for Na^+ transport mechanism by a light-driven Na^+ pump. Nature. 2015, 521, 48-53.

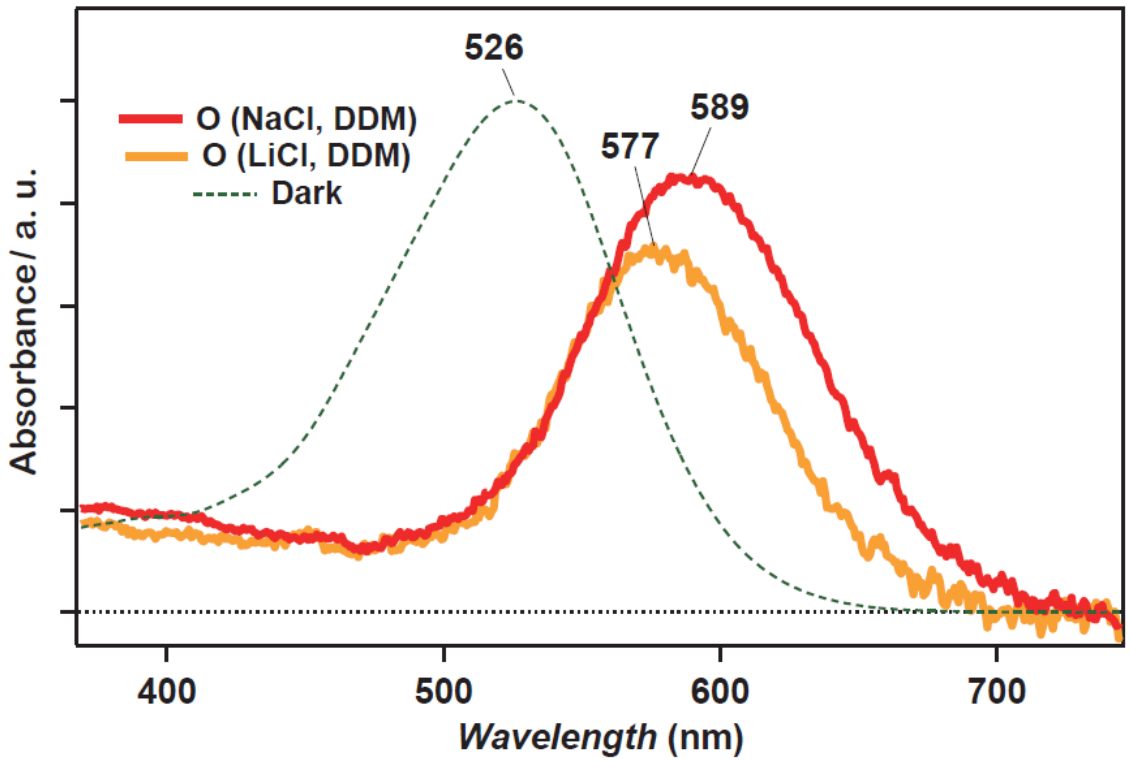

Figure S.2-13 Calculated absorption spectra of WT KR2 in the O intermediate state.

The absorption spectra of O intermediate of KR2 WT in the solution containing NaCl (red) or LiCl (yellow), calculated from the previously reported spectra[27]. The green dotted line represent the dark absorption spectrum of WT KR2 in the solution containing NaCl. The number above each spectrum is the peak wavelength (λ_{max}).

Chapter 3

Kinetic Analysis of H^+ - Na^+ Selectivity in a Light-Driven Na^+ Pumping Rhodopsin

3-1 Introduction

Ion selective mechanism is one of important topics of ion transport proteins because numerous ions exist in physiological bulk solution. Especially, the conduction of H^+ which is the smallest ion is difficult topics. H^+ conduction should be prevented because there are many H^+ (or pH) sensitive proteins. In water, the mobility of H^+ is ca. 7 times faster than that of Na^+. But, many selective cation channels prevent H^+ conduction by constructing cation selective pore. The hydrophilic pore of ion transport protein should constructed by hydrophilic group of amino acids such as hydroxyl, carbonyl, amid group etc. And, the pore often contain water molecules. H^+ translocation can occur via hydrogen bond network formed among amino acids and water molecules. For selective cation transport, such H^+ translocation should be prevented. In this study, we focus on H^+-Na^+ selectivity of light-driven sodium pump, KR2. KR2 pumps Na^+ in presence of Na+. It also pumps H^+ in the absence of Na^+ and Li^+. In previous studies, we mainly reveal Na^+ transport mechanisms because Na^+ is abundant in ocean where KR2 gene was discovered. We also obtain the insight that KR2 Q123V mutant transport both of H^+ and Na^+ in presence of Na^+. The simplest model which explain the result is H^+-Na^+ competitive uptake model. Na^+ and H^+ may be taken up competitively in this mutant. Wild type KR2 should behave same manner at low Na+ concentration. Here, we examine this hypothesis.

During the photoreaction of KR2 in NaCl, red-shifted K, blue-shifted L/M and red-shifted O intermediates sequentially appear.[2,7,20] In previous study, we concluded that Na^+ uptake

occurs in the L/M-to-O transition as the O formation was accelerated at high NaCl concentration.[7] This conclusion has been also supported by other groups on NaR from *Gillisia limnaea* (GLR).[10] According to the previous measurement, similar photointermediates are formed during the H^+ pump photoreaction in KCl, but the O accumulation was small.[7] Therefore, in the present study, we observed the M (L/M) intermediate in a concentration dependence study of H^+ and Na^+. We measured transient absorption change at 420 nm (corresponding to the M intermediate) after excitation of KR2 with a nanosecond-pulsed Nd^{3+}-YAG laser (λ = 532 nm).

3-2 Materials and Methods

Heterologous expression, purification and reconstitution of KR2

KR2 having six histidines at the C terminus were expressed in *E. coli.* C41(DE3) strain. The protein was purified via Co^{2+}-NTA affinity column (TALON, Qiagen) chromatography in manner previously described.[S1,S2] Purified sample was reconstituted into 1-palmitoyl-2-oleoyl-phosphatidylethanolamine (POPE, 16:0-18:1 PE, Avanti Polar Lipids, Inc.) and 1-palmitoyl-2-oleoyl-sn-glycero-3-phosphoglycerol (POPG-Na, COATSOME MG-6081LS, NOF ltd.) mixture lipid (molecular ratio was POPE:POPG = 3:1, KR2:Lipid = 1:20) by using biobeads. Reconstituted KR2 was washed ten times by using salt free buffer (20 mM Tris-H_3PO_4, 0 μM NaCl). After washing, sample suspension were sonicated. NaCl concentration was adjusted by adding NaCl buffer (20 mM Tris-H_3PO_4, 4 mM - 4 M NaCl). The samples were equilibrate over 30 min after adjusted NaCl concentration.

Flash photolysis

The transient absorption change of KR2 were monitored by flash photolysis as described previously.[3] The sample was illuminated with a beam of second harmonics of a nanosecond pulsed Nd^{3+}−YAG laser (λ = 532 nm, INDI40, Spectra-Physics), whose repetition rate was sufficiently slower than the photocycle rate to avoid photoexcitation of transient intermediates. The change in absorption after laser excitation was probed by monochromated light from the output of an Xe arc lamp (L9289−01, Hamamatsu Photonics, Japan), and the change in intensity of the probe light passed through the sample was monitored by a photomultiplier tube (R10699, Hamamatsu Photonics). The signal from the photomultiplier tube was averaged and stored by a digital-storage-oscilloscope (DPO7104, Tektronix, Japan). All measurement were at room temperature.

3-3 Results

Fig. 1a shows that the M decay is accelerated at high [NaCl], which is consistent with previous.[7] Fig. 1b shows the result in the absence of Na^+, and the M decay is also accelerated at high $[H^+]$ (low pH). This result indicates that not only Na^+ uptake but also H^+ uptake occurs upon the M decay. In M intermediate, Schiff base is deprotonated. And, Schiff base is re-protonated during the M decay transition. In the case of H^+ pump reaction, Schiff base receive proton from the bulk solution. In the case of Na^+ pump, Na^+ is taken up from bulk solution, the Na^+ uptake induce back H^+ transfer from protonated D116 to deprotonated Schiff base. The transient Na+ binding site is constituted by N112, D116, and D251, near Schiff base.[10,14] Although the detail mechanism and the terminal binding sites are different between H^+ and Na^+ uptake, probable reaction scheme and rate equation can be described as follows:

Scheme 1. Suggested reaction scheme of KR2

$$\mathrm{KR2} \longrightarrow\longrightarrow \mathrm{L/M} \begin{array}{l} \xrightarrow{k_{Na}[Na^+]} \mathrm{O_{Na}} \longrightarrow \\ \xrightarrow{k_{H}[H^+]} (\mathrm{O_H}) \longrightarrow \end{array} \mathrm{KR2}$$

$$[M] = [M]_0 \exp(-(k_{Na}[Na^+] + k_H[H^+]))$$

$$k_{obs} = k_{Na}[Na^+] + k_H[H^+]$$

k_{Na} and k_H represent the rate constants of Na^+- and H^+-uptake pathway, respectively. The solid measurement by using pH indicator also showed that H^+ uptake correlates well the M to O transition in GLR in the absence of sodium.[10] And, The H^+- and Na^+-dependent branches on M intermediate was also suggested in GLR, although H^+ uptake thought to occur extracellular side because net H^+ transport was not observed in GLR.[10]

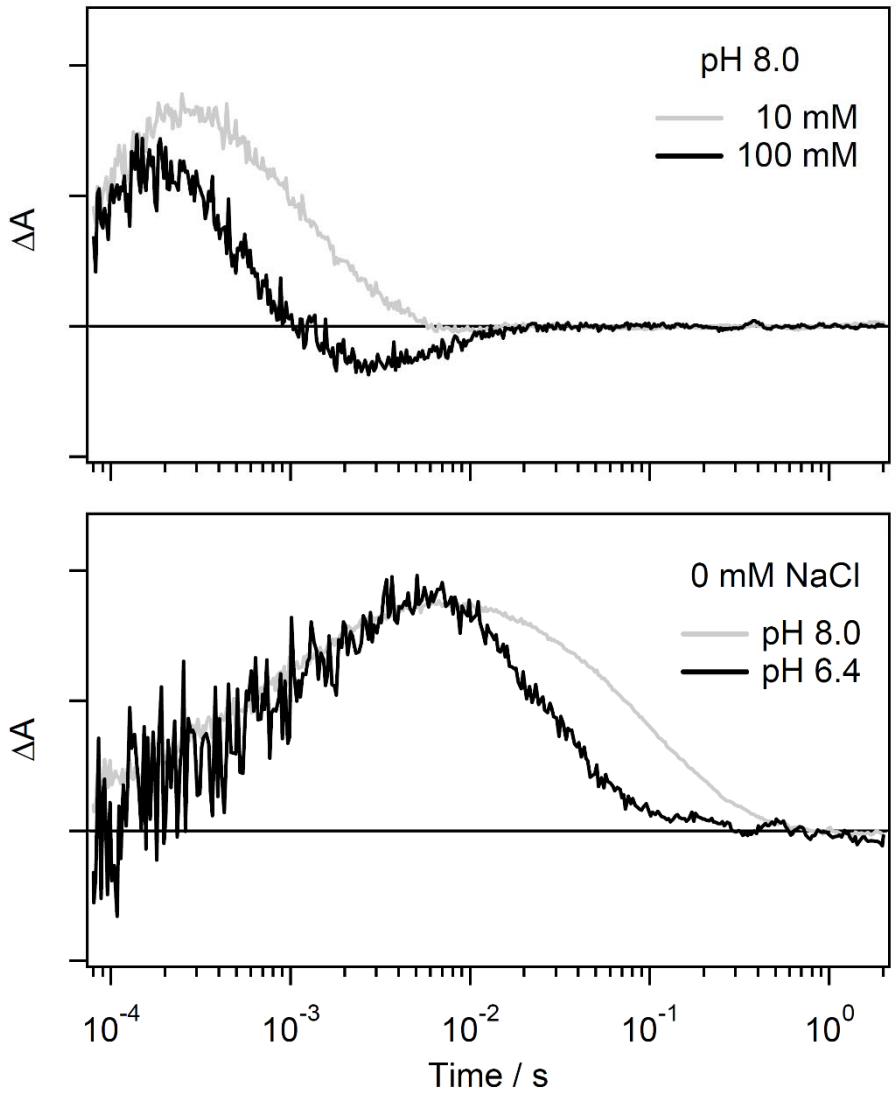

Figure 3-1. NaCl- and pH-dependence of M intermediate.

The absorption change at 420 nm was measured. (a) Time evolutions in 10 mM (gray line) and 100 mM (black line) NaCl at pH 8.0. (b) Time evolutions at pH 8.0 (gray line) and pH 6.4 (black line) in the absence of NaCl. Traces of pH 6.4 were normalized to those at pH 8.0. One division of the y-axis corresponds to 0.005 absorbance units.

In order to examine the suitability of the competitive uptake scheme, we further measured the time evolutions of M intermediate among a wide range of [NaCl]; 0 and 1 μM to 100 mM at three different pH (Figure 3-2). The M decay was fitted by single or double exponential curve. A significant acceleration of M decay was observed at >10 μM NaCl, but was not observed within a range of 0 to 10 μM NaCl at pH 8.0. This may be attributed to the fact that $k_{Na}[Na^+]$ is much smaller than $k_H[H^+]$ at ≤10 μM. At pH 7.0 and 6.4, the acceleration was observed at ≥1 mM and at ≥10 mM, respectively. It should be noted that the kinetic changes during the rise in M were also observed, though the shift was much smaller than that of M decay, and the effective concentration range was relatively higher (>100 μM at pH 8.0). From the perspective of effective concentration range, such kinetic changes during the rise in M may be related to the extracellular sodium binding site, which was identified in the dark state.[7] The dissociation constant (K_d) of the extracellular sodium binding site is 11.4 mM at pH 8.0, but this site is not necessary for Na^+ transport.[7]

Initial states at pH 7.0 and 6.4 are a mixture of two forms (Fig. S1) that are related to the protonation state of D116, which is the counter ion of the protonated Schiff base. This might complicate the analysis. However, photocycles of the wild-type KR2 at low pH and the KR2 D116N mutant do not contain any blue-shifted intermediates.[7] Furthermore, the D116N mutant cannot transport any ions,[7] which is also the case for the wild-type KR2 at low pH. Considering these results, the photocycle of the acidic form possessing the protonated D116 should not affect the present analysis.

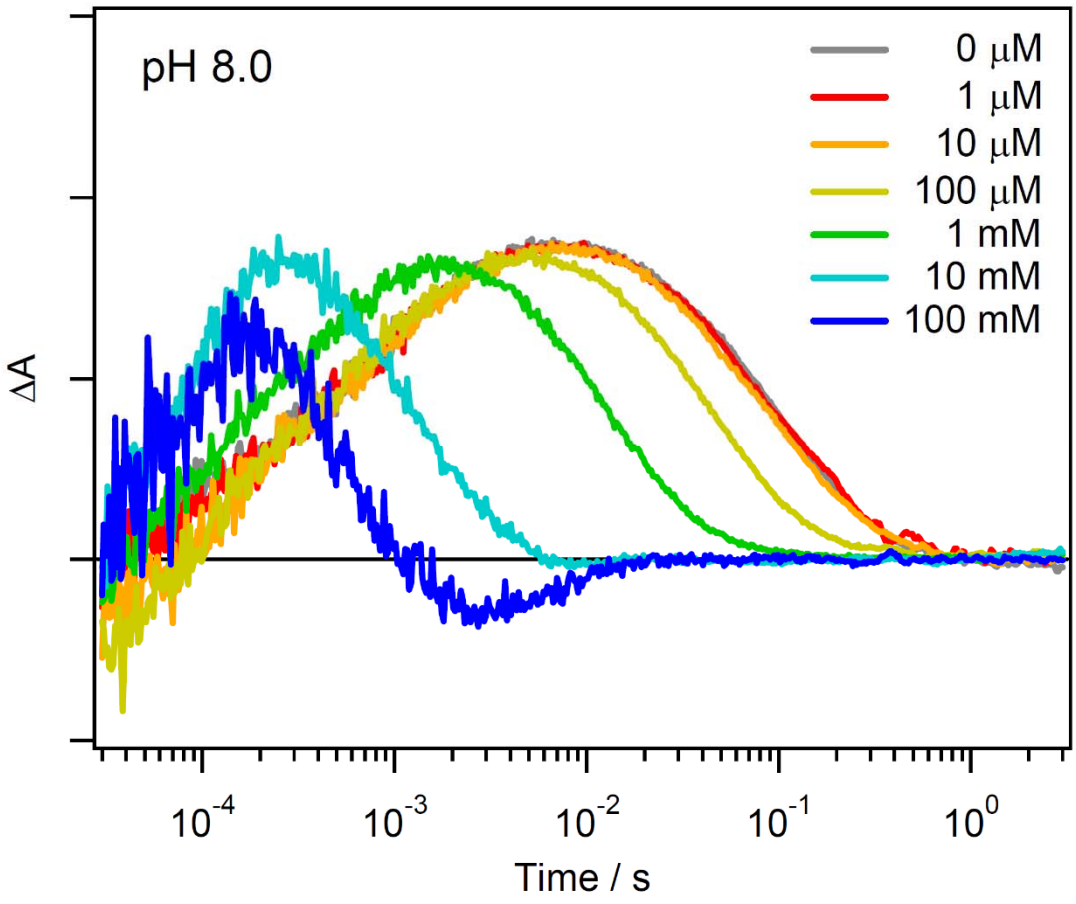

Figure 3-2. Na^+-dependence of the kinetics of the M intermediate.

Time traces of the change in absorption at 420 nm were measured in several NaCl concentrations at pH 8.0 (a). One division of the y-axis corresponds to 0.005 absorbance units.

Subsequently, the time constant of the M decay was plotted against [NaCl] to quantitatively investigate H^+ - Na^+ selectivity (Fig. 3). According to the competitive H^+ - Na^+ uptake model, selectivity during the uptake transition (k_H/k_{Na}) can be expressed as:

$$\tau = \frac{1}{k_{Na} \times \left([Na^+] + \frac{k_H}{k_{Na}} [H^+] \right)} \quad (1)$$

Fig. 3 shows that M decay becomes faster at a high Na^+ concentration at each pH, where the ion that has been taken up is converted from H^+ to Na^+. Good fitting curves in Fig. 3-3 demonstrate that the M decay kinetics can be described by a simple model of competitive uptake of Na^+ and H^+. After fitting with equation (1), the value of k_H/k_{Na} at pH 8.0, 7.0 and 6.4 was determined to be 8700, 8600 and 7200, respectively. Furthermore, we calculated the midpoint NaCl concentration (C_M) at which 50 % of KR2 take Na^+ up. The value of C_M was 90 μM at pH 8.0. In a previous study on GLR, the midpoint of Na^+ concentration at which the Na^+ pump feature was observed was calculated by another analysis (~60 μM).[10] H^+ transport was not observed in GLR. This value is very close to the C_M of KR2 determined in the present study. The C_M value increases at lower pH: 900 μM at pH 7.0 and 3 mM at pH 6.4. This shift resulted from the competition between H^+ and Na^+.

The present results are summarized in Fig. 3-4. Photoactivated KR2 is first converted to the K intermediate, which contains a 13-*cis* retinal.[2] In this state, protein does not recognize which ions will be transported as indicated by identical structural changes.[9] K is converted to the L/M intermediate equilibrium state. Ion uptake occurs upon decay of L/M. According to the present kinetic analysis of various Na^+ and H^+ concentrations, H^+ - Na^+ selectivity is represented by the ratio of the rate constants, k_H/k_{Na}. The value was determined to be 7000-9000 at around neutral pH, using the scheme in this study. It should be noted that the present

scheme postulates the M decay only originating from H^+ and Na^+ uptake from aqueous phase. However, under low H^+ and Na^+ concentrations, M decay could occur by internal H^+ donor, which could deviate the present analysis. In fact, the formula (1) predicts that in the absence of Na^+, the time constant of M decay should decrease 10 fold when pH is changed from 8 to 7. Comparison of red and green circles at 0 M NaCl in Fig. 3-3 shows the value to be < 3, indicating that contribution of internal H^+ donor cannot be negligible under such conditions. Therefore, to determine the k_H/k_{Na} value precisely, we need the third kinetic component from internal H^+ donor, for which M decay should be measured at wide pH range in the absence of Na^+. While it is our future focus, the present analysis using the formula (1) is sufficient to estimate the k_H/k_{Na} value to be $>10^3$ for KR2 from the analysis in Figs. 3-2 and 3-3.

Balashov et al. reported similar competitive H^+ and Na+ uptake for GLR under low Na+ concentration.[10] It is however noted that GLR does not pump H^+, and the observed event for GLR was interpreted as H^+ uptake as the extracellular side, followed by H^+ release at the same side (more precisely, one H^+ release first, then two H^+ uptake, and one H^+ release). Although H^+ uptake from the extracellular side for KR2 cannot be excluded at present, H^+ transport activity observed in KR2 strongly suggests H^+ uptake exclusively taking place at the cytoplasmic side (Fig. 3-4).

From the k_H/k_{Na} value ($>10^3$), KR2 takes up H^+ much more efficiently than Na^+ under the same concentration. On the other hand, KR2 actually takes up Na+ dominantly under physiological conditions, because [Na+] is 5×10^7 times larger than [H^+] in the ocean ([Na^+] and [H^+] are about 0.5 and 1×10^{-8} M, respectively). The intracellular Na^+ and H^+ concentrations of marine bacteria are different and 70 mM Na^+ at pH 7.6 ~ 7.8.[21,22] Even in this case, KR2 predominantly takes up Na^+.

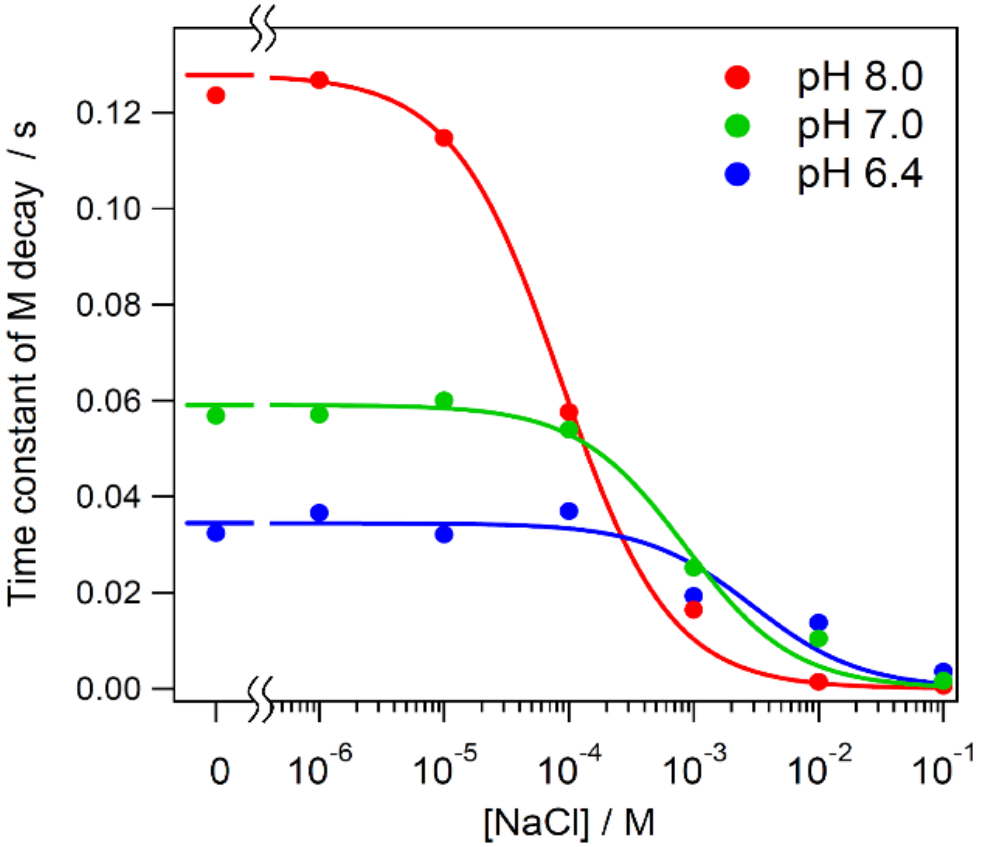

Figure 3-3. Calculation of H^+ - Na^+ selectivity during ion uptake transition.

Time constants of the M decay were plotted against NaCl concentration (filled circle). Solid curves indicate fitting curves represented by equation (1).

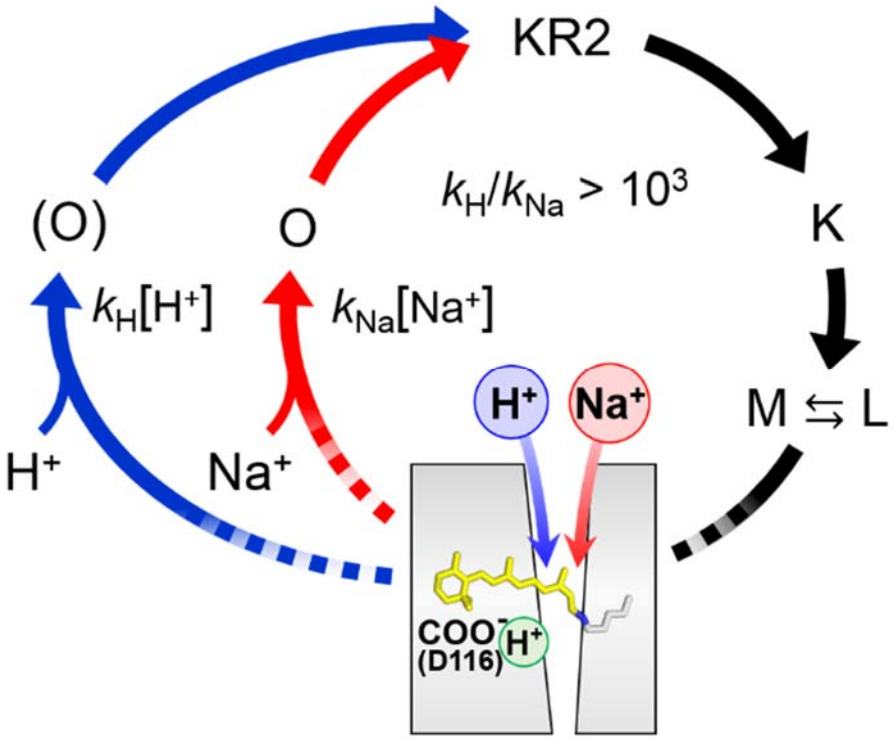

Figure 3-4. Kinetic scheme of the competitive ion uptake model.

Uptake of Na^+ and H^+ occurs during M decay. The rate constants of Na^+ and H^+ uptake are represented by k_H and k_{Na}, respectively. The value of the "k_H/k_{Na}" ratio is $>10^3$ at pH 6.4 - 8.0.

3-4 Discussion

It is intriguing to compare the permeability of H+ and Na+ in ion-transporting membrane proteins such as channels, transporters and flagella motor complexes.23 The permeability ratio (P_H/P_{Na}) for the amiloride-sensitive Na^+ channel and the voltage-gated Na+ channel (Na_v) is 7~25 and 252~274, respectively.[24,25] On the other hand, the P_H/P_{Na} of the voltage-gated proton channel (H_{v1}) is ≥ 10^6.[26] Since the value for ChR2 is ~10^6,[16] ChR2 should be recognized as a light-gated H^+ channel rather than an Na^+ channel. The selectivity for KR2 is intermediate between Na^+ and H^+ transporting machineries. The obtained k_H/k_{Na} value (10^3) does not represent the permeability across the membrane (P_H/P_{Na}), rather for the half channel on the cytoplasmic side. In addition, the terminal acceptor after uptake is the Schiff base for H^+, and the transient Na^+ binding site near Asn112 and Asp251.[10,14] Therefore, binding affinity to each site may influence the k_H/k_{Na} value. In this sense, Na^+ transport is less advantageous as the transient Na^+-binding site is located on the extracellular side.[10,14] This might raise the KR2 k_H/k_{Na} value.

In the case of BR, Asp96 acts as the internal H^+ donor to the Schiff base, and its mutation significantly slows down the reprotonation of the Schiff base (M decay).[27-29] In the case of many eubacterial H^+ pump rhodopsins, glutamate at the corresponding position acts as the internal H^+ donor.[30,31] The corresponding residue in the Na+ pump KR2 is glutamine (Gln123), which cannot be the internal H^+ donor. Interestingly, Gln123 optimizes Na^+ uptake because the Q123V mutation largely decreases Na^+ transport activity.[14] The selectivity filter of Na^+ is located around Asn61 and Gly263 at the cytoplasmic surface, whose mutation created a light-driven K^+ pump.[8,12] Therefore, the uptake pathway is comprised of a selectivity filter near Asn61 and Gly263 at the entrance, a hydrophobic interior containing Gln123, and a terminal acceptor site. Structural dynamics upon decay of the M intermediate determined the

observed k_H/k_{Na} value.

BR is a well-oknown outward H^+ pump. However, about 15 years ago, an interesting hypothesis was proposed that BR may not be an outward H+ pump but rather an inward OH^- pump. The idea was based on the structural observation of water movement from the Schiff base to the cytoplasmic region in the M intermediate of BR.[32] This raised an important question about the mechanism of the H^+ pump. An outward H^+ pump can be achieved by (i) outward H^+ transport, (ii) outward H_3O^+ transport, (iii) inward OH^- transport, or (iv) the Grotthuss mechanism[33] (concerted H^+ transfer through water chains). Functional conversion of BR into a Cl^- pump by a single amino acid replacement[34] was interpreted as supporting evidence of BR being an inward OH^- pump.[32,35] However, discovery of a light-driven Na^+ pump allows this scenario to be reconsidered, even though the OH^- pump hypothesis has never been experimentally denied for BR. The Grotthuss mechanism most likely takes place in light-driven H^+-pumping rhodopsins,[36] including the present case, and the competitive uptake will be further studied theoretically and experimentally. In summary, the present study established a competitive H^+ - Na^+ uptake model for KR2, and its H^+ - Na^+ selectivity (k_H/k_{Na}) was determined to be $>10^3$. Despite higher H^+ conduction than that for Na^+, this value is sufficient for NaR to function as a Na+ pump under physiological conditions.

REFERENCES

(1) Ernst, O. P.; Lodowski, D. T.; Elstner, M.; Hegemann, P.; Brown, L. S.; Kandori, H. Microbial and Animal Rhodopsins: Structures, Functions, and Molecular Mechanisms. *Chem. Rev.* **2014**, *114*, 126-163.

(2) Kandori, H. Ion-Pumping Microbial Rhodopsins. *Front. Mol. Biosci.* **2015**, 2, 52.

(3) Oesterhelt, D.; Stoeckenius, W. Rhodopsin-Like Protein from the Purple Membrane of *Halobacterium Halobium*. *Nat. New Biol.* **1971**, *233*, 149-152.

(4) Béjà, O.; Aravind, L.; Koonin, E. V.; Suzuki, M. T.; Hadd, A.; Nguyen, L. P.; Jovanovich, S. B.; Gates, C. M.; Feldman, R. A.; Spudich, J. L.; *et al.* Bacterial Rhodopsin: Evidence for a New Type of Phototrophy in the Sea. *Science* **2000**, *289*, 1902-1906.

(5) Venter, J. C.; Remington, K.; Heidelberg, J. F.; Halpern, A. L.; Rusch, D.; Eisen, J. A.; Wu, D.; Paulsen, I.; Nelson, K. E.; Nelson, W.; *et al.* Environmental Genome Shotgun Sequencing of the Sargasso Sea. *Science* **2004**, *304*, 66-74.

(6) Rusch, D. B.; Halpern, A. L.; Sutton, G.; Heidelberg, K. B.; Williamson, S.; Yooseph, S.; Wu, D.; Eisen, J. A.; Hoffman, J. M.; Remington, K., et al. The Sorcerer II Global Ocean Sampling Expedition: Northwest Atlantic through Eastern Tropical Pacific. *PLoS Biol*. **2007,** *5*, e77.

(7) Inoue, K.; Ono, H.; Abe-Yoshizumi, R.; Yoshizawa, S.; Ito, H.; Kogure, K.; Kandori, H. A Light-Driven Sodium Ion Pump in marine bacteria. *Nat. Commun.* **2013**, *4*, 1678.

(8) Kato, H. E.; Inoue, K.; Abe-Yoshizumi R.; Kato, Y.; Ono, H.; Konno, M.; Hososhima, S.; Ishizuka, T.; Hoque, M. R.; Kunitomo, H.; *et al.* Structural Basis for Na^+ Transport Mechanism by a Light-Driven Na^+ Pump. *Nature* **2015**, *521*, 48-53.

(9) Ono, H.; Inoue, K; Abe-Yoshizumi, R.; Kandori, H. FTIR Spectroscopy of a Light-driven Compatible Sodium Ion-Proton Pumping Rhodopsin at 77 K. *J. Phys. Chem. B* **2014**, *118*, 4784-4792.

(10) Balashov, S. P.; Imasheva, E. S.; Dioumaev, A. K.; Wang, J. M.; Jung, K. H.; Lanyi J. K. Light-Driven Na^+ Pump from *Gillisia Limnaea*: a High-Affinity Na^+ Binding Site is formed Transiently in the Photocycle. *Biochemistry* **2014**, *53*, 7549-7561.

(11) Inoue, K.; Kandori, H. Na^+ Transport by a Sodium Ion Pump Rhodopsin is resistant to Environmental Change: A Comparison of the Photocycles of the Na^+ and Li^+ Transport Processes. *Chem. Lett.* **2015**, *44*, 294-296.

(12) Gushchin, I.; Shevchenko, V.; Polovinkin, V.; Kovalev, K.; Alekseev, A.; Round, E.; Borshchevsky, V.; Balandin, T.; Popov, A.; Gensch, T.; *et al.* Crystal Structure of a Light-Driven Sodium Pump. *Nat. Struct. Mol. Biol.* **2015**, *22*, 390-395.

(13) da Silva, G.F.; Goblirsch, B. R.; Tsai, A. L.; Spudich, J. L. Cation-Specific Conformations in a Dual-Function Ion-pumping Microbial Rhodopsin. *Biochemistry* **2015**, *54*, 3950-3959.

(14) Inoue, K.; Konno, M.; Abe-Yoshizumi, R.; Kandori, H. The Role of the NDQ Motif in Sodium-Pumping Rhodopsins. *Angew. Chem. Int. Ed.* **2015**, 54, 11536-11539.

(15) Li, H.; Sineshchekov, O. A.; da Silva, G. F.; Spudich, J. L. In Vitro Demonstration of Dual Light-Driven Na^+/H^+ Pumping by a Microbial Rhodopsin. *Biophys. J.* **2015**, *109*, 1446-1453.

(16) Nagel, G.; Szellas, T.; Huhn, W.; Kateriya, S.; Adeishcili, N.; Berthold, P.; Ollig, D.; Hegemann, P.; Bamberg, E. Channelrhodopsin-2, a Directly Light-Gated Cation-Selective Membrane Channel. *Proc. Nat. Acad. Sci. USA* **2003**, *100*, 13940-13945.

(17) Deisseroth, K.; Optogenetics. *Nat. Methods* **2011**, 8, 26-29.

(18) Hegemann, P.; Möglich, A. Channelrhodopsin Engineering and Exploration of New Optogenetic Tools. *Nat. Methods* **2011**, *8*, 39-42.

(19) Beppu, K.; Sasaki, T.; Tanaka, K. F.; Yamanaka, A.; Fukazawa, Y.; Shigemoto, R.; Matsui, K. Optogenetic Countering of Glial Acidosis Suppresses Glial Glutamate Release and Ischemic Brain Damage. *Neuron* **2014**, *81*, 314-320.

(20) Inoue, K.; Kato, Y.; Kandori, H. Light-Driven Ion-Translocating Rhodopsins in Marine Bacteria. *Trends Microbiol.* **2015**, *23*, 91-98.

(21) Padan, E.; Bibi, E.; Ito, M.; Krulwich, T. A. Alkaline pH Homeostasis in Bacteria: New insights. *Biochim. Biophys. Acta.* **2005**, *1717*, 67-88.

(22) Nakamura, T.; Kawasaki, S.; Unemoto, T.; Roles of K^+ and Na^+ in pH Homeostasis and Growth of the Marine Bacterium *Vibrio Alginolyticus*. *J. Gen. Microbiol.* **1992**, *138*, 1271-1276.

(23) DeCoursey, T. E. Voltage-gated proton channels: Voltage-Gated Proton Channels: Molecular Biology, Physiology, and Pathophysiology of the H_v Family. *Physiol. Rev.* **2013**, *93*, 599-652.

(24) Mozhayeva, G. N.; Naumov, A. P. The Permeability of Sodium Channels to Hydrogen Ions in Nerve Fibres. *Pflugers Arch.* **1983**, *396*, 163-173.

(25) Gilbertson, T. A.; Avenet, P.; Kinnamon, S. C.; Roper, S. D. Proton Currents through Amiloride-Sensitive Na Channels in Hamster Taste Cells. Role in Acid Transduction. *J. Gen. Physiol.* **1992**, *100*, 803-824.

(26) Demaurex, N.; Grinstein, S.; Jaconi, M.; Schlegel, W.; Lew, D. P.; Krause, K. H. Proton Currents in Human Granulocytes: Regulation by Membrane Potential and Intracellular pH. *J. Physiol.* **1993**, *466*, 329-344.

(27) Otto, H.; Marti, Y.; Holz, M.; Mogi, T.; Lindau, M.; Khorana, H. G.; Heyn M. P. Aspartic Acid-96 is the Internal Proton Donor in the Reprotonation of the Schiff Base of Bacteriorhodopsin. *Proc. Natl. Acad. Sci. USA* **1989**, *86*, 9228-9232.

(28) Holz, M.; Drachev, L. A.; Mogi, T.; Otto, H.; Kaulen, A. D.; Heyn, M. P.; Skulachev, V. P.; Khorana H. G. Replacement of Aspartic Acid-96 by Asparagine in Bacteriorhodopsin Slows both the Decay of the M Intermediate and the Associated Proton Movement. *Proc. Natl. Acad. Sci. USA.* **1989**, *86*, 2167-2171.

(29) Gerwert, K.; Hess, B.; Soppa, J.; Oesterhelt, D. Role of Aspartate-96 in Proton Translocation by Bacteriorhodopsin. *Proc. Natl. Acad. Sci. USA.* **1989**, *86*, 4943-4947.

(30) Dioumaev, A. K.; Brown, L. S.; Shih, J.; Spudich, E. N.; Spudich, J. L.; Lanyi, J. K. Proton Transfers in the Photochemical Reaction Cycle of Proteorhodopsin. *Biochemistry* **2002**, *41*, 5348-5358.

(31) Miranda, M. R.; Choi, A. R.; Shi, L.; Bezerra, A. G. Jr.; Jung, K. H.; Brown L. S. The Photocycle and Proton Translocation Pathway in a Cyanobacterial Ion-pumping Rhodopsin. *Biophys. J.* **2009**, *96*, 1471-1481.

(32) Luecke, H. Atomic Resolution Structures of Bacteriorhodopsin Photocycle Intermediates: the Role of Discrete Water Molecules in the Function of This Light-Driven Ion Pump. *Biochim. Biophys. Acta* **2000**, *1460*, 133-156.

(33) Agmon, N. The Grotthuss Mechanism. *Chem. Phys. Lett.* **1995**, *244*, 456-462.

(34) Sasaki, J.; Brown, L. S.; Chon, Y. S.; Kandori, H.; Maeda, A.; Needleman, R.; Lanyi, J. K. Conversion of Bacteriorhodopsin into a Chloride Ion Pump. *Science* **1995**, *269*, 73-75.

(35) Facciotti, M. T.; Rouhani, S.; Glaeser, R. M. Crystal Structures of bR(D85S) Favor a Model of Bacteriorhodopsin as a Hydroxyl-Ion Pump. *FEBS Lett.* **2004**, *564*, 301-306.

(36) Freier, E.; Wolf, S.; Gerwert, K. Proton Transfer via a Transient Linear Water-Molecule Chain in a Membrane Protein. *Proc. Natl. Acad. Sci. USA* **2011**, *108*, 11435-11439.

Chapter 4

Mutant of a Light-Driven Sodium Ion Pump Can Transport Cesium Ions

4-1 Introduction

A light-driven outward H+ pump converts light energy into a proton motive force, which is used to synthesize ATP.[1-5] A light-driven inward Cl^- pump also creates a membrane potential for ATP-synthesis.[4] The light-driven H^+ pump bacteriorhodopsin (BR)[6] and the Cl^- pump halorhodopsin (HR)[7-8] were discovered from Halophilic archaea. Since 2000, metagenomic analysis revealed that ion-pumping rhodopsins are widely distributed among marine prokaryotes, most of which were classified as light-driven H^+ pumps or proteorhodopsin (PR).[9] It is now believed that half of marine bacteria contain light-driven ion-pumping rhodopsins, with new and significant contributions of rhodopsin phototrophy having been identified in the marine environment.[10-11] In addition, these rhodopsins are important tools for neural silencing in optogenetics.[12,13] Thus, light-driven ion-pumping rhodopsins have attracted much interest recently.

Compared to light-driven H^+ and Cl^- pumps, the discovery of a light-driven Na^+ pump was relatively novel.[14] All microbial rhodopsins possess an all-trans retinal as the chromophore, which binds to a lysine residue through a protonated retinal Schiff base (SB) linkage.[4] As the chromophore is positively charged, it was believed that non-proton cations such as Na^+ could not be bound near the protonated SB because of an electrostatic repulsion, and thus Na^+ transport was thought to be impossible. Therefore, finding light-driven outward Na^+ pumping rhodopsins (NaRs) raised various questions about the mechanism. NaRs are able to pump Na^+ outwardly, but cannot pump K^+.[14] This fact suggests the presence of a selective filter that is larger than Na^+ (radius: 1.94 Å) but smaller than K^+ (radius: 2.82 Å).

Where is the selectivity filter located in NaR? It is reasonable to consider the location near the retinal SB, because vectorial transport is determined by the SB region, where SB works as the switch.[4] It is also reasonable to consider that the Na^+ pathway must be sufficiently narrow at the middle of the protein, because SB is embedded on the putative Na^+ transport pathway. However, recent structure-guided molecular engineering studies revealed that KR2 mutants G263F and N61P/G263W function as a K^+ pump.[15-16] This observation strongly suggests that the selectivity filter of cations is located at the cytoplasmic surface, and in fact, N61 and G263 constitute the narrowest cavity in the uptake pathway of cations.[15-16] In this structure, the distance between the side-chain oxygen/nitrogen of N61 and Cα of G263 is 4.0-5.9 Å,[15-16] which could be permeable to K^+. This suggests that the cavity becomes even more narrow upon cation uptake during the KR2 photocycle and may be related to a puzzling result in which the transport of a larger cation (K^+) was achieved by introducing larger amino acids, which may have narrowed the cavity. There are many questions related to the selectivity of cations in KR2.

In the present study, we introduced several mutations such as bulky amino acids into positions 61 and 263 of KR2 to better understand the selectivity filter in NaR. One of the goals of this study was to create a Cs^+ pump, the machinery to transport larger monovalent cations. Unlike the K^+ pump, the Cs^+ pump is not in demand in optogenetics, because Cs^+ is not abundant in our brain. However, there are no light-driven Cs^+ pumps in nature. Therefore, creation of light-driven Cs^+ pump will open many possibilities, including collection of $^{137}Cs^+$ by light which could be used in the Fukushima nuclear power plant..

4-2 Materials &Methods

Synthesized KR2 gene was optimized for *E.coli* expression system based on the sequence from Krokinobacter eikastus NBRC 100814T（Genbank protein ID：BAN14808.1）. KR2, which has six histidine residues at the C-terminus, was expressed in the *E. coli* C41 (DE3) strain. Amino acids mutation was introduced to positions 61 and 263 on KR2 using PCR-based site-directed mutagenesis (QuikChange site-directed mutagenesis kit, Stratagene). The protein-induced cells were washed once, equilibrated for 10 minutes three times and resuspended with 100 mM solution at each salt condition for equilibration of ion condition inside cells. Cell suspensions were illuminated for 150 seconds at wavelength > 500 nm with 1-kW tungsten-halogen projector lamp (Master HILUX-HR, Rikagaku, Japan) through a glass filter (Y-52, AGC Techno Glass, Japan). The light-induced pH changes during the incubation were monitored with a pH meter (F-55, Horiba, Japan). Measurements were repeated under the same conditions after the addition of 10 mM CCCP. The amount of protein was estimated by the bleaching of KR2 by hydroxylamine. The values of ion pumping activity were corrected with the protein expression level in *E.coli* cell.

4-3 Results

Fig. 4-1 summarizes the pump activity of Na^+, K^+ and Cs^+, where a positive signal represents the transport of each cation, while a negative signal originates from the H^+ pump. The WT pumps Na^+ outwardly, but pumps neither K^+ nor Cs^+, indicating that the size of the selectivity filter is smaller than K^+. Three mutants, N61W, N61L/G263W, and N61Y/G263W, exhibited no pump activity at all, because no pigment formed. Introduction of bulky groups at the 61-263 region could prevent proper protein folding. Among the N61 mutants, N61Y gains K^+ pump activity as we reported previously.[15] N61Y seems to have weak Cs^+ pump activity in the light, because a pH increase was observed when the competing H^+ transport was eliminated by CCCP (see Table 4-1).. Both G263 mutants (G263F and W) show clear K^+ pump activity. In addition, G263F shows Cs^+ pump activity, although the efficiency is much lower than for Na^+ and K^+. We then tested a combination of mutations at position 61 and 263. Although N61Y and G263F both show weak Cs^+ pump activity, N61Y/G263F and N61P/G263F do not pump Cs^+. On the other hand, N61L/G263F pumps Cs^+ most efficiently ($KR2_{Cs+}$), and reaches 12 % of the Na+ pump and 60 % of the K^+ pump in the presence of CCCP (Table 4-1). We previously reported that N61P/G263W ($KR2_{K+}$) pumps K^+ more efficiently than Na^+.[15] Nevertheless, N61P/G263W does not pump Cs^+ at all, and no Cs^+ pump activity was observed for single and double mutants containing G263W.

Fig. 4-2 shows the volume dependence of light-driven ion pump activity. Na^+ pump activity does not depend on the volume of position 61 and 263, but the activity in the presence of CCCP is gradually lowered as the volume increases (Figure 4-2a). In the case of the K^+ pumping activity, the initial slope of ion-transport rate tends to become positive (indicated K^+ pumping) from a negative (indicated H^+ pumping) by increasing the volume, with an approximate linear fit (Figure 4-2b). The most efficient K^+ pump is N61P/G263W ($KR2_{K+}$),[15]

which is more efficient than G263W, N61P/G263F, and G263F (Table 1).

Table 4-1. Initial slope of pump activity in positions 61 and 263 of KR2 mutants.

Protein	Volume[a] (61) (cm^3 mol^{-1})	Volume[a] (263) (cm^3 mol^{-1})	Volume (61+263) (cm^3 mol^{-1})	Initial slope (mol H^+out s^{-1} mol^{-1} protein)					
				NaCl		KCl		CsCl	
				-CCCP	+CCCP[b]	-CCCP	+CCCP[b]	-CCCP	+CCCP[b]
WT	69.6	34.8	104.4	0.72	2.22	-0.27	-0.11	-0.54	-0.15
N61P	72.6	34.8	107.4	0.22	1.47	-0.38	-0.19	-0.57	-0.21
N61L	99.1	34.8	133.9	0.67	1.85	-0.16	0.05	-0.34	-0.12
N61Y	114.7	34.8	149.5	0.70	2.05	0.07	0.56	-0.08	0.05
G263F	69.6	112.8	182.4	0.53	1.24	0.18	0.61	-0.02	0.14
N61P/G263F	72.6	112.8	185.4	0.67	1.60	0.28	0.81	-0.02	0.05
G263W	69.6	135.5	205.1	0.57	1.54	0.20	0.93	-0.03	0.03
N61P/G263W ($KR2_{K+}$)	72.6	135.5	208.1	0.14	0.85	0.33	1.03	0.06	0.06
N61L/G263F ($KR2_{Cs+}$)	99.1	112.8	211.9	0.45	1.49	0.07	0.31	0.03	0.18
N61Y/G263F	114.7	112.8	227.5	0.49	1.48	0.09	0.30	-0.05	0.02

[a]The volume of residues as indicated by Zamyatnin (1984)[17].

[b]10 μM CCCP was added into *E. coli* cell suspension.

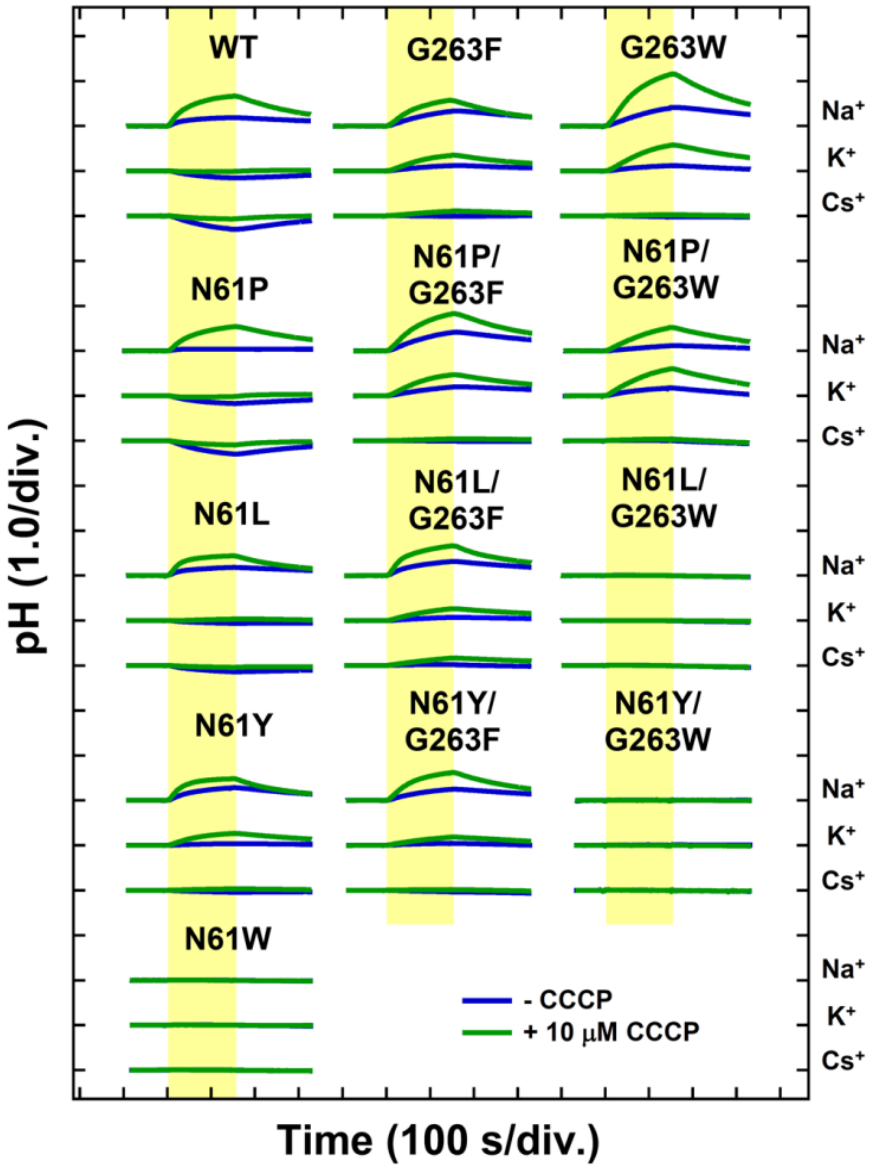

Figure 4-1. Pump activities of KR2 WT and mutants in E. coli cells suspended in 100 mM NaCl (top), KCl (middle) or CsCl (bottom), without (blue) and with (green) 10 μM CCCP. N61L/G263W, N61Y/G263W and N61W are colourless mutants. Yellow shading indicates the period of light illumination, i.e., 150 seconds.

The calculated volume of the residues KR2K^+ at positions 61 and 263 is 208.1 cm^3mol^{-1}, which is two-fold larger than in WT (Table 4-1). We infer that bulky amino acids have been introduced into the selectivity filter possibly destroying the local structure, which affected the light-induced conformational change in the opening state, thus creating an enlarged cavity. It should be noted that a volume larger (210-230) than $KR2_{K+}$ again lowers the activity (Figure 4-2b). In addition, when volume is further enlarged at this region, no pigment forms, such as in N61L/G263W (234.6 cm^3mol^{-1}) and N61Y/G263W (250.2 cm^3mol^{-1}). Thus, the local structure of this region seems to be crucial for both ion selectivity and protein stability. Since any structures of reactive intermediate of KR2 isn't known at present, the precise size of the filter couldn't be revealed. Therefore, the measurement of the size of the filter will be next issue in further study.

Volume dependence is also clearly seen for the Cs^+ pump (Figure 4-2c), where H^+ pump activity is significantly reduced when the volume is increased to 100-160 $cm^{-3}mol^{-1}$. This does not originate from the emergence of the Cs^+ pump, because there is no positive signal with CCCP in this region. Figure 4-2b and c show that it is difficult to transport Cs^+ compared to K^+, presumably because Cs^+ is larger than K^+. $KR2_{Cs+}$ clearly pumps Cs^+ in the presence of CCCP, while pump activity is unclear in its absence (Figures 4-1 and 4-2). This suggests that $KR2_{Cs+}$ pumps H^+ which competes with Cs^+ in CsCl. We conclude that $KR2_{Cs+}$ makes a large entrance cavity for Cs^+ uptake at the transition from the M to the O intermediate,[14, 18] although it is competing with H^+ uptake. KR2 WT exclusively pumps Na^+ in NaCl, and H^+ in KCl and CsCl.[14] On the other hand, we recently reported that KR2 Q123V pumps Na^+ and H^+ in NaCl in a competing manner,[19] presumably because of significantly slowed Na^+ uptake. This suggests a common transport mechanism for Na^+, H^+ and Cs^+, where the selection of ions is determined by kinetic factors in the cytoplasmic domain.

We then systematically compared the ion-pump activity of $KR2_{Cs+}$ in LiCl, NaCl, KCl, RbCl and CsCl. In WT, Li^+ transport was 65 % of Na^+ transport,[20] and did not transport K^+, Rb^+, and Cs^+. This indicates the strict size-dependence of the selectivity filter, which is probably located at N61 and G263 in the cytoplasmic surface. Except for Li^+, the ion-transport rate is negative correlation to the dehydrated ionic radii. The result suggested that the ions are dehydrated when they are transported via KR2. It is considered that the dehydration penalty of ions was compensated with the coordination of the amino acid residues near the ion-selective filter. The ionic diameters of Li^+, Na^+, K^+, Rb^+ and Cs^+ are 1.42, 1.94, 2.82, 3.00, and 3.46 Å, respectively,[21] and if dehydrated ions permeate through the selectivity filter, pore size is located between 1.94 and 2.82 Å. On the other hand, $KR2_{Cs+}$ transports all monovalent cations, and the efficiency of Li^+ relative to Na^+ (45 %) is lower than in WT (65 %) (Figure 4-3). Thus, the size of the selectivity filter pore seems to have broadened by mutation. In parallel, it seems that ion selectivity is lower, suggesting that the $KR2_{Cs+}$ pore structure fluctuates more. The introduction of bulky amino acids probably affects the helical opening structure at about positions 61 and 263. In EPR study, the TM7 helix showed light-induced movement to outside of the protein[22]. Since there is G263 on TM7 helix, we considered that the replacement of this residue to bulky amino acid could induce the helix opening even in dark state, and TM7 helix movement of K^+- or Cs^+-pumping mutants are larger than WT. To gain further details of ion-transport mechanism, we investigated the photocycle of $KR2_{Cs+}$ in 100 mM NaCl or CsCl. We focused the recovery of initial state of KR2 protein. The KR2 recovery rate in CsCl was approximately 5-folds slower than that in NaCl. This result is consistent with the ion-transport rate in CsCl (12%), which was slower than the rate in NaCl (Figure 4-3).

4-4 Discussion

The permeability of monovalent cations inside a protein has been extensively studied for ion channels.[23] In the case of Gramicidin A channels that possess a pore of 4 Å in diameter and about 25 Å long, ionic permeability is $Li^+ < Na^+ < K^+ \leq Rb^+ < Cs^+$, being more permeable for larger cations.[24] Therefore, if we are able to create a larger entrance at the cytoplasmic surface, a more efficient Cs^+ pump could be designed in the future. The present study demonstrates that light can be used for the unidirectional transport of Cs^+. One application is the collection of Cs^+ by forming reverse vesicles, which has already been established.[25] Thus, in the future, $KR2_{Cs+}$ may be used to collect leaked $^{137}Cs^+$ at the Fukushima nuclear power plant. To achieve this aim, the efficiency and ion-selectivity of $KR2_{Cs+}$ have to be improved.

In summary, the creation of $KR2_{K+}$ was enabled by a structure-based functional design.[15] We have now extended the functional design to $KR2_{Cs+}$. The volume dependence of the residues at 61 and 263 was linearly correlated with the transport activity of K^+ and Cs^+, suggesting that the ion-selectivity filter is located in this region. The selectivity filter strictly excludes K^+ (and Cs^+), but introduction of large residues possibly destroys local structures of the ion-selectivity filter, leading to the permeation of K^+ (P61/W263) and Cs^+ (L61/F263). This first light-driven Cs^+ pump offers many possibilities for applications in the future.

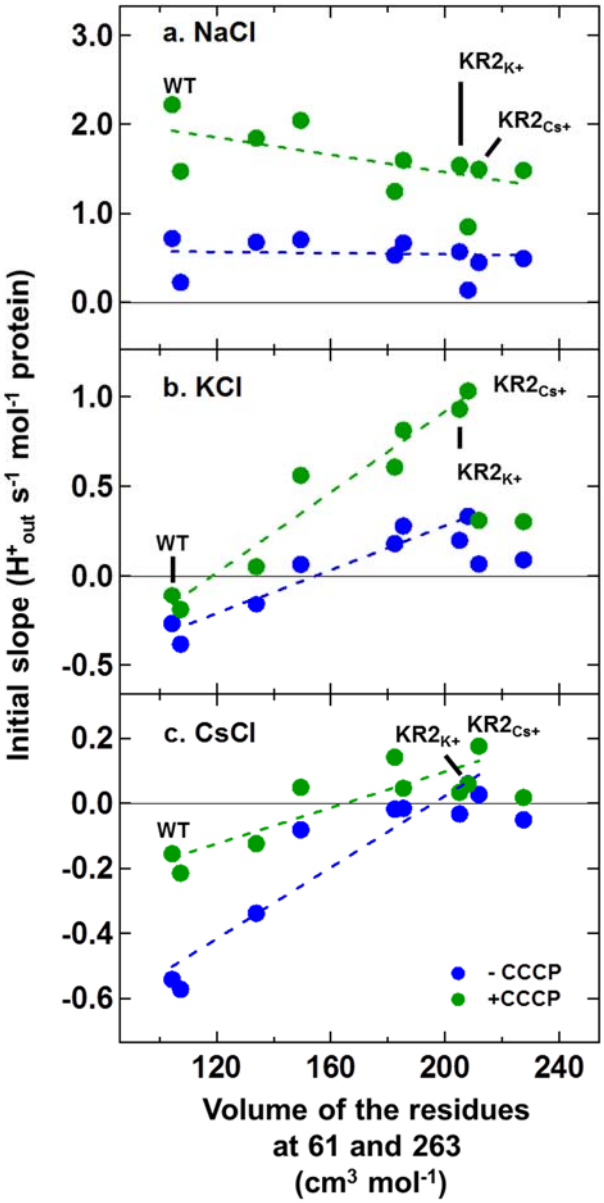

Figure 4-2. Correlation between pumping activity and the additive volume of the amino acid residues at positions 61 and 263 in KR2. Blue and green filled circles represent the initial slope in each pump without and with CCCP, respectively.

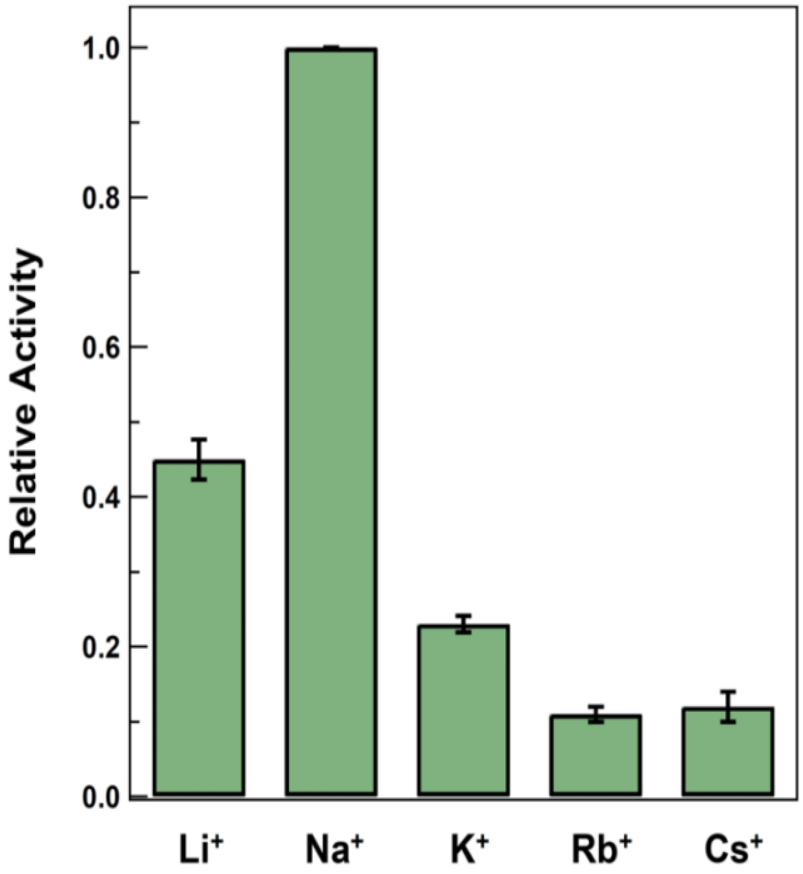

Figure 4-3. Pump activities of $KR2_{Cs+}$ in E. coli cells suspended in 100 mM LiCl, NaCl, KCl, RbCl, and CsCl.

REFERENCES

1. Racker, E.; Stoeckenius, W. Reconstitution of Purple Membrane Vesicles Catalyzing Light-driven Proton Uptake and Adenosine Triphosphate Formation. *Journal of Biological Chemistry* **1974,** *249* (2), 662-663
2. Haupts, U.; Tittor, J.; Oesterhelt, D. Closing in on Bacteriorhodopsin: Progress in Understanding the Molecule. *Annu. Rev. Biophys. Biomol. Struct.* **1999**, 28, 367-399.
3. Lanyi, J. K. Halorhodopsin: A Light-driven Chloride Ion Pump. *Annu. Rev. Biophys. Biophys. Chem.* **1986**, 15 (1), 11-28.
4. Ernst, O. P.; Lodowski, D. T.; Elstner, M.; Hegemann, P.; Brown, L. S.; Kandori, H. Microbial and Animal Rhodopsins: Structures, Functions, and Molecular Mechanisms. *Chem. Rev.* **2014**, 114 (1), 126-163.
5. Kandori, H. Ion-Pumping Microbial Rhodopsins. Front. Mol. Biosci. **2015**, 2, 52.
6. Oesterhelt, D.; Stoeckenius, W. Rhodopsin-like Protein from the Purple Membrane of *Halobacterium halobium*. *Nat.New Biol.* **1971**, 233 (39), 149-152.
7. Matsuno-Yagi, A.; Mukohata, Y. Two Possible Roles of Bacteriorhodopsin; a Comparative Study of Strains of *Halobacterium halobium* Differing in Pigmentation. *Biochem. Biophys. Res. Commun.* **1977**, 78 (1), 237-243.
8. Schobert, B.; Lanyi, J. K. Halorhodopsin is a Light-Driven Chloride Pump. *J. Biol. Chem.* **1982,** *257* (17), 10306-10313.
9. Béjà, O.; Aravind, L.; Koonin, E. V.; Suzuki, M. T.; Hadd, A.; Nguyen, L. P.; Jovanovich, S. B.; Gates, C. M.; Feldman, R. A.; Spudich, J. L.; et al. Bacterial Rhodopsin: Evidence for a New Type of Phototrophy in the Sea. *Science* **2000**, 289 (5486), 1902-1906.

10. Moran, M. A.; Miller, W. L. Resourceful Heterotrophs Make the Most of Light in the Coastal Ocean. *Nat. Rev. Microbiol.* **2007**, 5 (10), 792-800.

11. de la Torre, J. R.; Christianson, L. M.; Beja, O.; Suzuki, M. T.; Karl, D. M.; Heidelberg, J.; DeLong, E. F. Proteorhodopsin Genes Are Distributed Among Divergent Marine Bacterial Taxa. *Proc. Natl. Acad. Sci. USA* **2003**, 100 (22), 12830-12835.

12. Gradinaru, V.; Zhang, F.; Ramakrishnan, C.; Mattis, J.; Prakash, R.; Diester, I.; Goshen, I.; Thompson, K. R.; Deisseroth, K. Molecular and Cellular Approaches for Diversifying and Extending Optogenetics. *Cell* **2010**, 141 (1), 154-165.

13. Han, X.; Chow, B. Y.; Zhou, H.; Klapoetke, N. C.; Chuong, A.; Rajimehr, R.; Yang, A.; Baratta, M. V.; Winkle, J.; Desimone, R.; et al. A High-Light Sensitivity Optical Neural Silencer: Development and Application to Optogenetic Control of Non-Human Primate Cortex. *Front. Syst. Neurosci.* **2011**, 5, 18.

14. Inoue, K.; Ono, H.; Abe-Yoshizumi, R.; Yoshizawa, S.; Ito, H.; Kogure, K.; Kandori, H. A Light-Driven Sodium Ion Pump in Marine Bacteria. *Nat. Commun.* **2013**, 4, 1678.

15. Kato, H. E.; Inoue, K.; Abe-Yoshizumi, R.; Kato, Y.; Ono, H.; Konno, M.; Ishizuka, T.; Hoque, M. R.; Hososhima, S.; Kunitomo, H.; et al. Structural Basis for Na^+ Transport Mechanism by a Light-Driven Na^+ Pump. *Nature* **2015**, 521 (755), 48-53.

16. Gushchin, I.; Shevchenko, V.; Polovinkin, V.; Kovalev, K.; Alekseev, A.; Round, E.; Borshchevskiy, V.; Balandin, T.; Popov, A.; Gensch, T.; et al. Crystal Structure of a Light-Driven Sodium Pump. *Nat. Struct. Mol. Biol.* **2015**, 22 (5), 390-395.

17. Zamyatnin, A. Amino acid, Peptide, and Protein Volume in Solution. *Annu. Rev. Biophys. Bioeng.* **1984**, 13 (1), 145-165.

18. Balashov, S. P.; Imasheva, E. S.; Dioumaev, A. K.; Wang, J. M.; Jung, K.-H.; Lanyi, J. K. Light-Driven Na^+ Pump from *Gillisia limnaea*: A High-Affinity Na^+ Binding Site Is Formed Transiently in the Photocycle. *Biochemistry* **2014**, 53 (48), 7549-7561.

19. Inoue, K.; Konno, M.; Abe-Yoshizumi, R.; Kandori, H. The Role of the NDQ Motif in Sodium-Pumping Rhodopsins. *Angew. Chem. Int. Ed.* **2015**, 127 (39), 11698-11701

20. Inoue, K.; Ono, H.; Kandori, H. Na^+ Transport by Sodium Ion Pump Rhodopsin Is Resistant to Environmental Change -A Comparison of Photocycles of Na^+ and Li^+ Transport Processes. *Chem. Lett.* **2014**, 44 (3), 294-296.

21. Marcus, Y. Ionic Radii in Aqueous Solutions. *Chem. Rev.* **1988**, 88 (8), 1475-1498.

22. da Silva, G. F. Z.; Goblirsch, B. R.; Tsai, A.-L.; Spudich, J. L. Cation-Specific Conformations in a Dual-Function Ion-Pumping Microbial Rhodopsin. *Biochemistry* **2015,** *54* (25), 3950-3959.

23. Hill, B. Ion Channels of Excitable Membranes. Third Edition ed.; Sinauer Associates, Inc.: Massachusetts, **2001**.

24. Myers, V. B.; Haydon, D. A. Ion Transfer Across Lipid Membranes in the Presence of Gramicidin A: II. The Ion Selectivity. *Biochim. Biophys. Acta.* **1972**, 274 (2), 313-322.

25. Nishio, K.; Iwamoto-Kihara, A.; Yamamoto, A.; Wada, Y.; Futai, M. Subunit Rotation of ATP Synthase Embedded in Membranes: α or β Subunit Rotation Relative to the C Subunit Ring. *Proc. Nat. Acad. Sci.* **2002**, 99 (21), 13448-13452.

Chapter 5

Spectroscopic Study of a Light-Driven Chloride Ion Pump from Marine Bacteria

5-1 Introduction

In 1970s, light-driven proton pump (bacteriorhodopsin, BR) and chrolide pump (halorhodopsin, HR) were discovered from a halophilic archaea, *Halobacterium salinarum* (*Halobacterium halobium*).[1-4] These proteins has hepta-transmembrane helices and conject retinal to a Lysine residue of a helix (helix G). These protein family had been called “archaeal rhodopsin” in those days. After discoveries of these two light-driven ion pump, two other similar proteins which act as phototaxis sensor were found from same archaea (SRI and SRII). In 1980-1990, the homologous proteins were found from other halophilic archaea. *Natronomonas pharaonis* found from Egypt contained halorhodopsin homologue (NpHR). *Halobacterium sp. aus-1* found from Australia contained bacteriorhodopsin homologue (AR1). The amino acid identity between BR and AR1 is ca. 60 %. The amino acid identity between *Hs*HR and *Np*HR is ca. 50 %. Although the amino acid sequence of these proteins are different from BR and HR (*Hs*HR), these remain proton pump or chloride pump function. Light-driven proton pump and chloride pump have specific sequence motifs, “DTD” and “TSA” motifs, respectively. In the case of BR, the first “D” of “DTD” motif is D85 which act as counter ion and H+ acceptor of protonated Schiff base. “T” is T89 which locate in one turn upper side of D85. The second “D” is D96 which act as H+ donor of deprotonated Schiff base of M intermediate during the photocycle. These amino acids are well-conserved among H^+ pump rhodopsins (but, the second “D” is replaced to “E” in many eukaryotic H^+ pumps). In the case of chloride pumps, these three amino acid of BR are replaced to T, S, and A, respectively. T, S and some residues forms Cl^- binding site, and Cl- act as counter ion of protonated Schiff

base instead of D85 in BR. The chloride and proton transport mechanisms of these rhodopsins have been studied for about 40 years since its discovery. The spectroscopy have been made a great contributions in the rhodopsin study. In the case of BR and HR, X-ray crystallographic structures of initial and intermediate states were also revealed at atomic level resolution. These structures lead us to understand there molecular mechanisms. Based on these studies, it have been thought that these motif is responsible for their functions. Since 2000, numerous archaeal rhodopsin homologues were found also from Bacteria and Eukaryota domains by highly developed genomic analysis. Nowadays, the word “archaeal rhodopsin” is superseded by “microbial rhodopsin”. Although numerous genes which encode microbial rhodopsin were found from ocean in 2000-2012, most of these rhodopsins act as light-driven proton pump. Recently, two motifs, “NDQ” and “NTQ” were newly discovered from marine bacteria. An NDQ rhodopsin, *Krokinobacter eikastus* rhodopsin 2 (KR2) was identified as light-driven sodium pump. Here, we study an NTQ rhodopsin found from a marine bacteria, *Fulvimarina pelagi* (FR). We revealed that FR is light-driven chloride pump. The amino acid identity between FR and *Hs*HR is 23%. The amino acid identity between FR and *Np*HR is 26%. On the other hand, the amino acid identity between FR and KR2 is 33%. Although functions are different, amino acid sequence of FR is close to KR2 rather than HRs. This may be attributed to evolutional aspect. Microbial rhodopsins may evolutionally spread their functional varieties by arranging their sequences for a long time, on which two different chloride pumps were created. The comparison studies between novel NTQ and well-studied TSA chloride pumps should give us new insight about the chloride transport mechanism.

5-2 Materials & Methods

Protein Expression in E. coli and Purification.

The FR gene codons were optimized for *E. coli* expression system and synthesized (Eurofins Genomics Inc.). The synthesized gene were inserted into pET-vector with C-terminal 6x His-tag. The protein was expressed in the *E. coli* C41(DE3) strain, and was purified in a similar way previously described with modification of buffer contents optimized for FR purification.[12,16] The membranes were solubilized with 1.5% n-Dodecyl β-D-maltoside (DDM) for 6 h at 4ºC. The solubilized membrane was centrifuged (35,000 rpm, 60 min, 4ºC) and the supernatant was applied into a Co-affinity column (TALON, Qiagen).

Phylogenic Analysis.

A molecular phylogenetic analysis of rhodopsins was conducted by the Maximum Likelihood method. The evolutionary history was inferred by using the Maximum Likelihood method based on the JTT matrix-based model.[17] The percentage of trees in which the associated taxa clustered together is shown next to the branches. Initial tree(s) for the heuristic search were obtained by applying the Neighbor-Joining method to a matrix of pairwise distances estimated using the JTT model. The tree was drawn to scale, with branch lengths measured in the number of substitutions per site. The analysis involved 23 amino acid sequences. All positions with less than 95% site coverage were eliminated, that is, fewer than 5% alignment gaps, missing data, and ambiguous bases were allowed at any position. There were a total of 226 positions in the final dataset. Evolutionary analyses were conducted in MEGA6.[18]

Ion-Pump Activity Measurements.

Pump activity measurements were performed with a pH electrode for *E. coli* cells.[12] Overnight cell cultures were diluted 1:100 and cultures were grown in shaker flasks at 37 °C and 180 rpm. Cultured cells were collected by centrifugation, washed and suspended in a solvent containing 100 mM salt. The illumination light source was a 1 kW tungsten-halogen projector lamp with a Y-52 (Toshiba, Tokyo, Japan) long-pass filter to cut light whose wavelength was shorter than 500 nm.

Flash Photolysis.

The transient absorption spectra of FR were monitored by flash photolysis measurements using a multichannel detector as described previously.[12] For spectroscopic measurements, purified FR was reconstituted into lipid bilayers (1,2-dioleoyl-*sn*-glycero-3-phosphocholine, DOPC). To measure transient absorption changes of FR, the proteins was reconstituted in DOPC (molecular ratio: FR:DOPC = 1:20). The sample was illuminated with a beam of second harmonics of a nanosecond pulsed Nd^{3+}-YAG laser (λ = 532 nm, INDI40, Spectra-Physics), whose repetition rate was sufficiently slower than the photocycle rate to avoid photo-excitation of transient intermediates.

The change in absorption at 525 nm after laser excitation was probed by monochromated light from the output of an Xe arc lamp (L9289-01, Hamamatsu Photonics, Japan), and the change in intensity of the probe light passed through the sample was monitored by a photomultiplier tube (R10699, Hamamatsu Photonics).[12] The signal from the photomultiplier tube was averaged and stored by a digital-storage-oscilloscope (DPO7104, Tektronix, Japan).

5-3 Results

FR is a light-driven inward chloride-ion pump.

In order to examine the functions of FR, we applied the ion transport activity measurement using pH meter which is a general method for predict the function of microbial rhodopsin (Figure 5-1). In NaCl, the light-induced alkalization signal were observed. In the case of outward proton pump, the acidification signal should be observed, and CCCP (protonophore) cancel the signal because CCCP enhance H^+ permeability across the hydrophobic cell membrane. The alkalization signal of FR was enhanced with CCCP. This results indicates that the secondary proton movement occurs in response to a transmembrane electrochemical gradient. This is supported by the reduction in the signal with hydrophobic cation, TPP^+. Therefore, FR is a light-driven outward sodium pump or an inward chloride pump. We can distinguish these two functions by changing cation or anion of the salt. FR expressing *E. coli* cells also showed alkalization signal in CsCl. On the other hand, the signal decrease in NaI, $NaNO_3$, and Na_2SO_4. In previous study about light-driven outward sodium pump, KR2, we observed cation dependence. In NaCl, KR2 expressing *E. coli* cells suspension shows light-induced alkalization. This alkalization signals were observed in NaCl, NaBr, and Na_2SO_4, but not in KCl, RbCl and CsCl. From the anion dependence observed for FR, we conclude that FR is a light-driven inward chloride-ion pump. The previous study shows that alkalization signals of the nitrate ion is much lower than that of the chloride ion for *Hs*HR. But, alkalization signals of both ions is similar for *Np*HR.[12] The ion transport activity of FR seems to be similar to *Hs*HR rather than *Np*HR.

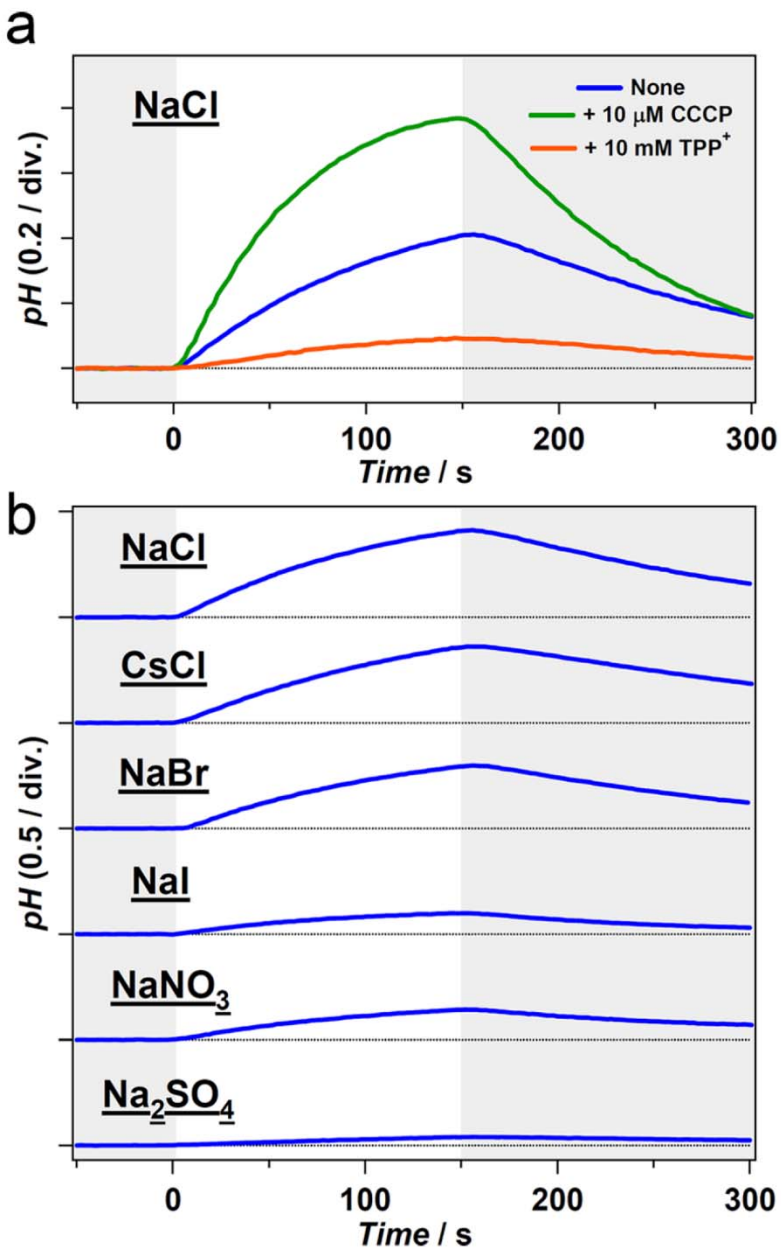

Figure 5-1 Pump activity of FR.

(a) Light-induced pH changes of the E. coli cells containing FR in 100 mM NaCl without (blue line) and with (green line) 10 mM CCCP. (b) Relative pumping activity of FR in the presence of 100 mM NaCl, CsCl, NaBr, NaI, $NaNO_3$ and Na_2SO_4, in which the protein concentration in E. coli cells is identical.

Chloride-ion binding to FR

KR2 showed no change in color between the presence and absence of sodium ions,[12] suggesting that the binding site is distant from the retinal chromophore. This view is consistent with the fact that the retinal chromophore is positively charged and sodium ion cannot bind near the chromophore because of electrostatic repulsion. On the other hand, chloride-ion pump HRs change color upon chloride-ion binding. Therefore, we measured the absorption spectra of FR under various salt conditions.

Figure 5-2a clearly shows salt-dependent absorption spectra in which chloride-ion binding caused a spectral blue shift. This property in FR is also similar to what was observed in *p*HR,[20] and well described by the color tuning mechanism in which a negatively charged chloride-ion localizes a positive charge at the Schiff base moiety, leading to the spectral blue shift upon chloride-ion binding.[1] FR absorption spectra depend on the concentration of salt, exhibiting a blue-shift with an isosbestic point at 527 nm. The difference spectra clearly demonstrates this blue-shift, which however was not saturated even at 1.66 M NaCl. From the titration results, a chloride ion is bound to FR with a dissociation constant (K_d) of 84.0 mM (Figure 5-2b). This value is much higher than for HR (3 mM),[20] indicating a lower affinity for chloride-ion binding for FR than for HR. Nevertheless, the binding affinity of the chloride ion to FR is probably sufficient under physiological conditions of the marine environment (chloride ion concentration of ~560 mM). The λ_{max} at 1.66 M NaCl does not correspond to the full binding of a chloride ion according to the titration curve in Figure 3c, and the calculated λ_{max} for the full binding was 515 nm (Table 5-1).

Figure S3 shows similar results for other anions such as the bromide ion, the iodide ion, and the nitrate ion. λ_{max} varies for different anions (Table 5-1), which also supports the notion that FR possesses an anion binding site near the retinal chromophore. The K_d value also

depends on anions (Table 5-1). Although the binding mechanism of an anion to the protein is similar between FR and *Np*HR, there is a noticeable difference in the halide-dependence on λ_{max}. There is little halide-dependence on the λ_{max} of *Np*HR (576, 578, and 577 nm for chloride, bromide, and iodide ions, respectively),[20] which is also the case for *Hs*HR (572, 575, and 571 nm for chloride, bromide, and iodide ions, respectively).[21] On the other hand, FR exhibits clear halide-size dependent changes in λ_{max}, where a spectral red-shift is observed for a large halide (Table 5-1). It should be noted that this tendency is the same for the λ_{max} in solution (460, 468, and 478 nm for chloride, bromide, and iodide ions, respectively).[22] This fact suggests that the local environment in FR is close to that in solution, in which the halide ion is probably the direct hydrogen-bonding acceptor of the Schiff base in FR, as well as in solution. Such an effect by the halide is masked in the binding pocket of HR. The X-ray structures of *Hs*HR and *Np*HR show that the Schiff base does not directly interact with a halide, but interacts through an internal water molecule.[20,23,24] Consequently, the hydrogen-bonding interaction between the Schiff base and chloride ion becomes weak, as evidenced by FTIR spectroscopy.[25] No direct interaction in HR probably leads to little halide dependence.

Table 5-1. The dissociation constant (K_d), λ_{max} of FR at 1.66 M salt concentration ($\lambda_{max, meas}$) and the calculated λ_{max} of the fully bound state of anion for FR ($\lambda_{max, calc}$).

	K_d (mM)	$\lambda_{max, meas}$ (nm)	$\lambda_{max, calc}$ (nm)
Cl^-	84 ± 4	518	515
Br^-	81 ± 5	520	517
I^-	44 ± 1	524	522
NO_3^-	129 ± 7	522	518

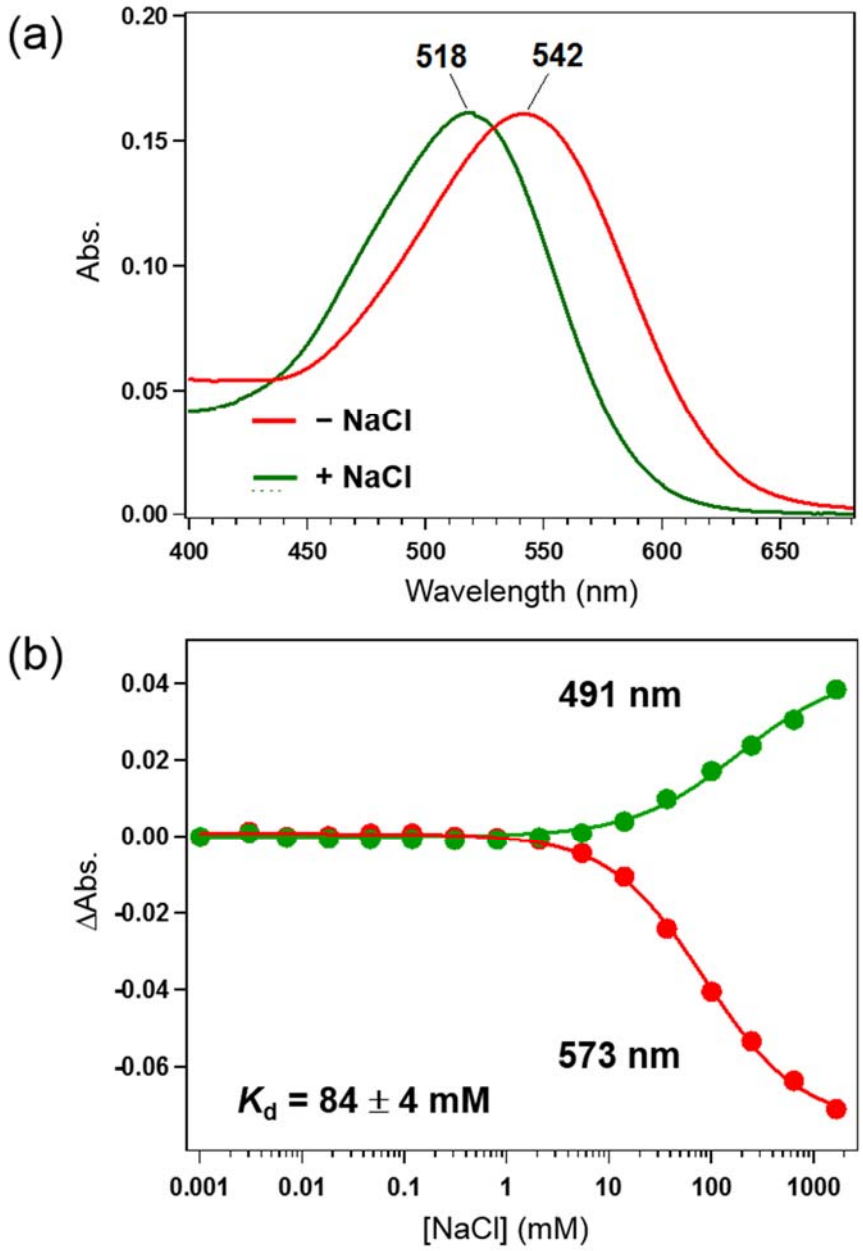

Figure 5-2 Chloride induced spectral changes of FR

(a) Absorption spectra of FR in a solvent containing 0 mM (green) and 1660 mM NaCl (red). (b) Absorption changes at the wavelengths of negative and positive peaks in difference spectra of (a). Solid lines indicate fitting curves using a Hill equation with n = 1.

Photocycle during chloride-ion pump in FR.

We next studied the photocycle during chloride-ion pumping, in which the FR protein is reconstituted into the lipid bilayer. Figure 5-3a shows the transient absorption spectra of FR from 80 μs to 69.2 ms, where a spectral red-shift was observed at all timescales (10^{-4} to 10^{-1} sec). No positive signals were observed at 350-450 nm, indicating no formation of the M intermediate. This is also the case for HR, and like HR, the Schiff base does not release a proton during the photocycle.[9] This is a common mechanism for the chloride-ion pump, in which the interaction changes between a positively charged retinal Schiff base and a negatively charged chloride ion which drives chloride-ion transport toward the cytoplasmic side.[1] Figure 5-3b shows typical kinetic traces in the photocycle of FR. While the transient absorption at 580-700 nm is positive at all timescales, the time-evolution of the absorption change at 589 nm was expressed by a double-exponential increase (τ = 250 μs and 2.6 ms) followed by a double-exponential decrease (τ = 3.7 μs and 20.4 ms) to the baseline. This is a characteristic feature of the O intermediate. In addition, we observed a decay at 575 nm at an earlier timescale, which was monitored only by single wavelength kinetic measurements (Figure 5-3d). The kinetics originate from the decay of the red-shifted K intermediate, whose time constant was 7.0 μs. The value is similar to that of the K intermediate of *p*HR (1.2 μs).[19] This observation suggests that the primary reaction of FR is the all-*trans* to 13-*cis* photoisomerization in an ultrafast timescale, which forms the primary K intermediate that decays to subsequent intermediates in an early μs regime.

From Figure 5-3a, spectral changes of FR appear monotonous, but the transient absorption spectra do not exhibit an isosbestic point, indicating that multiple kinetic processes are involved during the photocycle of the chloride ion pump. We thus applied singular value decomposition (SVD) analysis to these processes (Figure 5-3a). We then

obtained four kinetic components (0.25, 2.6, 3.7 and 20.4 ms) during the photocycle of FR (detailed analysis in Figure S5-4). Figure S5-4b and c show the time courses corresponding to the two largest singular values (V_1 and V_2) (see detailed explanation of SVD analysis in Supporting Information) and decay associated spectra (DAS) accompanying each of the four kinetic components, from which difference absorption spectra to the unphotolyzed FR (Figure S5-4c) were obtained. Using the difference spectra in Figure S5-4d, absolute absorption spectra of the intermediates were reconstituted (Figure 5-3c).

The spectra decay at 250 μs possess a peak at 526 nm with a broad feature at 550-700 nm, and we interpret the K and L intermediates, which are formed by the decay of the K intermediate in 7.0 μs, to be in equilibrium (Figure 5-3c). The second spectrum decay at 2.6 ms (orange curve in Figure 5-3c) is also broad, suggesting an equilibrium of at least two states. In contrast, the third spectrum decay at 3.7 ms (green curve in Figure 5-3c) possesses a sharp feature with the λ_{max} at 556 nm, and the spectral red-shift by 38 nm is characteristic of the O intermediate. As the second and third time constants (2.6 and 3.7 ms) are close to each other, we believe that the second component originated from the equilibrium between the L and O intermediates. The forth spectrum decay at 20.4 ms has a λ_{max} at 536 nm, which can be described by a mixture of the O intermediate (46 %) and original absorption (FR′ states, 54 %). Consequently, the photocycle of FR during the chloride ion pump can be summarized as follows.

$$\mathrm{FR} \xrightarrow{\text{light}} \mathrm{K} \xrightarrow{7.0\ \mu s} \mathrm{K/L} \xrightarrow{250\ \mu s} \mathrm{L/O} \xrightarrow{2.6\ \text{ms}} \mathrm{O} \xrightarrow{3.7\ \text{ms}} \mathrm{O/FR'} \xrightarrow{20.4\ \text{ms}} \mathrm{FR}$$

The HR photocycle has been extensively studied, and described as the K, L, and O intermediates as well as the presence of HR′ at the end of the photocycle.[19, 26-28] Therefore, the photocycle of FR closely resembles that of HR. In the case of HR, the existence of two L

intermediates (L_1 and L_2) was observed by various methods,[10, 25, 27-31] suggesting that there are accessbility changes between the extracellular and cytoplasmic sides, which is analogous to the M_1 and M_2 intermediates of BR.[1] An alteration in hydroben-bonding in the Schiff base region makes the vectorial transport of the chloride ion into the cytoplasmic side via the L_1 and L_2 intermediates possible,[21] and the chloride ion is released to the cytoplasmic side during the transition to the O intermediate.[26] Formation of the L states is a prerequisite for the chloride-ion pump because no L forms in HR in the absence of salt.[19] Chloride ion uptake is accompanied by the decay of the O intermediate which is accelerated at high salt concentrations.[19] Consequently, the O intermediate is not observed at high salt concentrations. We next examined how salt concentration affects the FR photocycle.

Salt concentration dependence of the FR photocycle.

While the earlier photocycle does not change under different salt conditions, Figure 5b clearly shows that O formation was accelerated at a high salt concentration. This indicates that the chloride ion is taken up at the stage between the L/O to O intermediate, and is entirely different from the results for HR. In the case of HR, the O intermediate resembles the chloride ion-free form, and the decay in O is similar to chloride-ion binding.[19] In contrast, the O intermediate of FR (λ_{max}: 556 nm) binds chloride ion inside the protein. Nevertheless, a greater red-shifted λ_{max} of the O intermediate than that of the chloride ion-free form (λ_{max}: 542 nm) suggests that the chloride ion does not bind to the Schiff base region, and that the binding site does not influence the color of FR. Thus, the transient formation of the chloride-ion binding site, presumably near the extracellular surface, is implicated for the late photocycle stage of FR. It should be noted that the decay in O is also

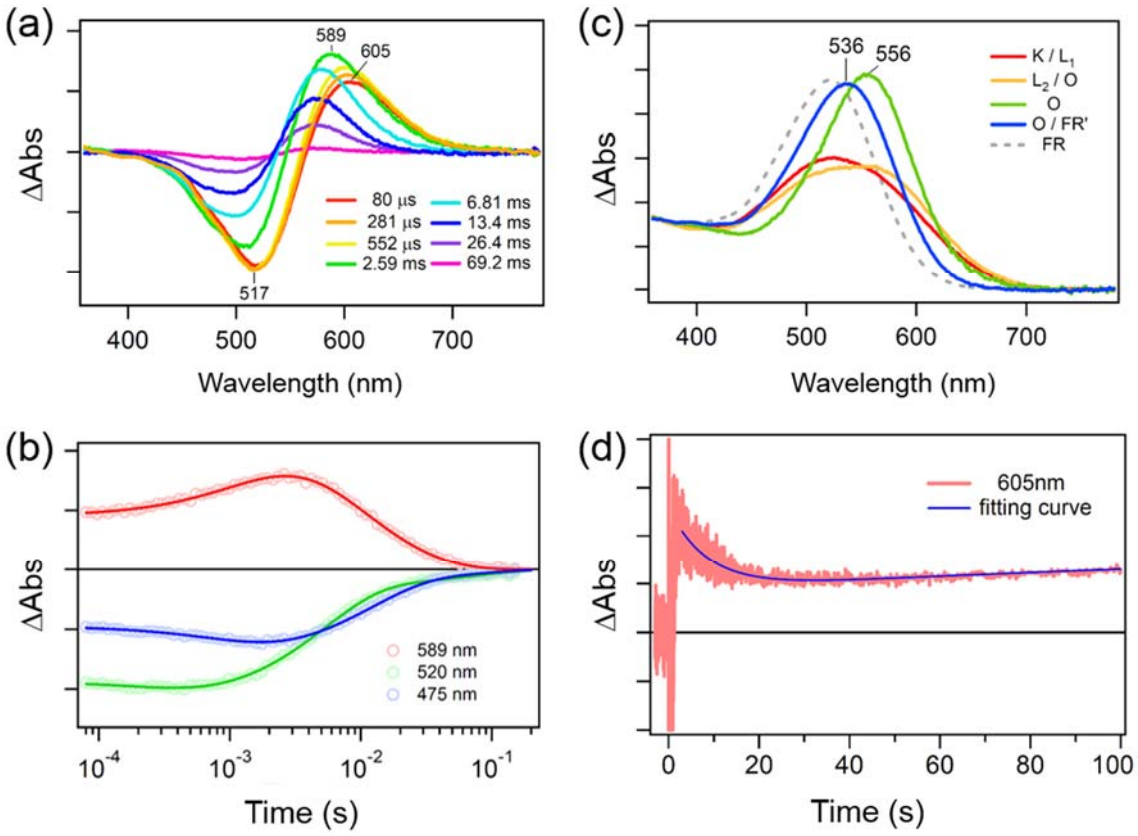

Figure 5-3 Photocycle using the chloride-ion pump of FR (100 mM NaCl).

(a) Transient absorption spectra of FR. (b) Time-evolution at specific wavelengths (475 nm, blue; 520 nm, green; 589 nm, red) from 80 μs to 150 ms. (c) Absolute absorption spectra of FR (dashed line) and its intermediates (solid lines) obtained by singular value decomposition analysis. (d) Time trace at 575 nm; the decay curve (red) is fitted by an exponential process of 7.0 μs (blue).

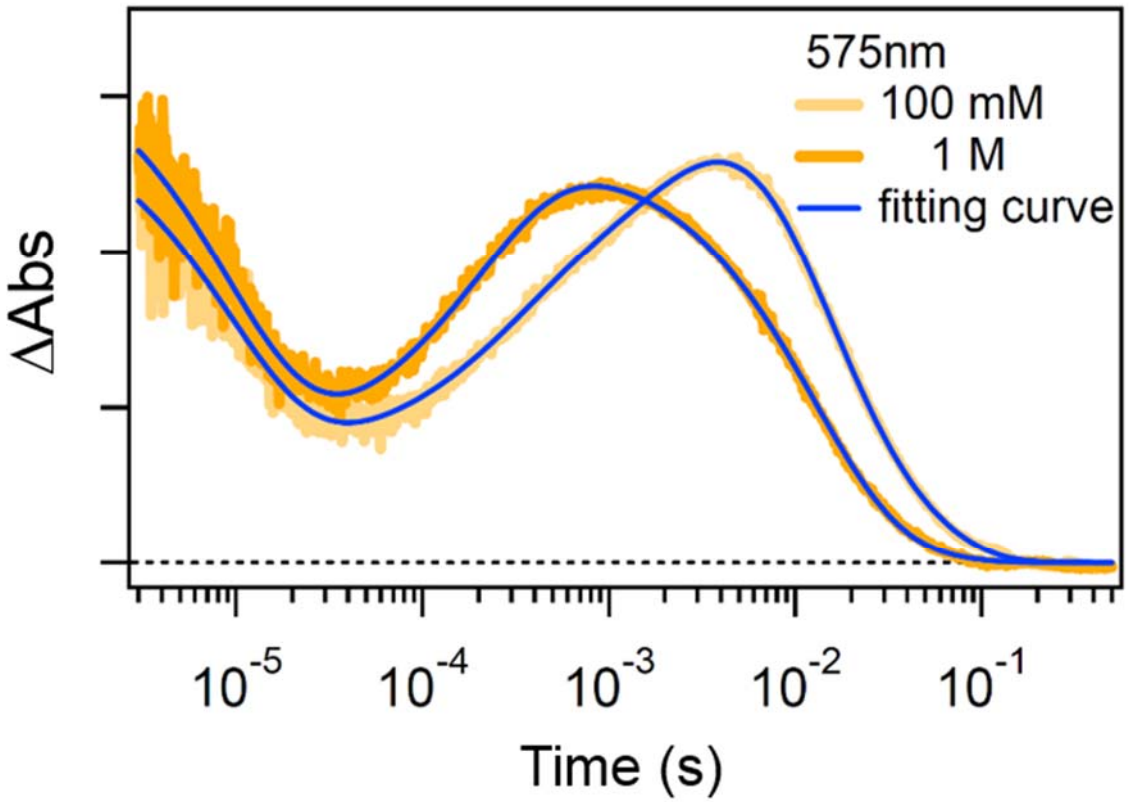

Figure 5-4　Salt concentration dependence of the FR photocycle.

Concentration dependence of chloride ions in the rise and decay kinetics of the O intermediate of FR. The absorption change was observed at two different NaCl concentrations, 100 mM (pale orange) and 1 M (thick orange) NaCl. To compensate the difference of ionic strength, 300 mM Na_2SO_4 was added to the former.

accelerated in FR at a high salt concentration (Figure 5-4). This is in clear contrast to the uptake of the sodium ion in KR2, where O only increases but is not decayed, and accelerated in the light-driven sodium-ion pump at a high salt concentration.[12] This suggests that uptake of the chloride ion also takes place upon the decay of O in FR.

Figure 5-5 shows transient absorption spectra of FR in the absence of NaCl. Spectral changes appear monotonous in which only a red-shifted intermediate appeared. It should be noted, however, that unlike the presence of NaCl, the transient absorption spectra exhibit an isosbestic point, indicating that the photocycle in the absence of salt is simpler than that during the chloride-ion pump, which can be summarized as follows.

$$\mathrm{FR(Cl^- free)} \xrightarrow{\text{light}} \text{K-like} \xrightarrow{<80\ \mu\text{s}} \text{O-like} \xrightarrow{1.0 \text{ and } 5.2 \text{ ms}} \text{FR}$$

Lack of the L intermediate in the photocycle of the chloride-free FR implies the functional importance of the L intermediate for the chloride-ion pump, which is also the case for HR.[19] A chloride ion binds to the Schiff base region of FR, which must be stabilized by a hydrogen-bonding network, and a hydroben-bonding alteration in the Schiff base region makes the vectorial transport of the chloride ion into the cytoplasmic side. Formation of the L intermediate is strongly coupled to this process. Identical results were obtained for FR in 33 mM Na_2SO_4 (Figure S5-4), in which neither anion binding nor transport occurred. They are consistent with the results in the absence of salt, because both FR do not bind an anion near the Schiff base.

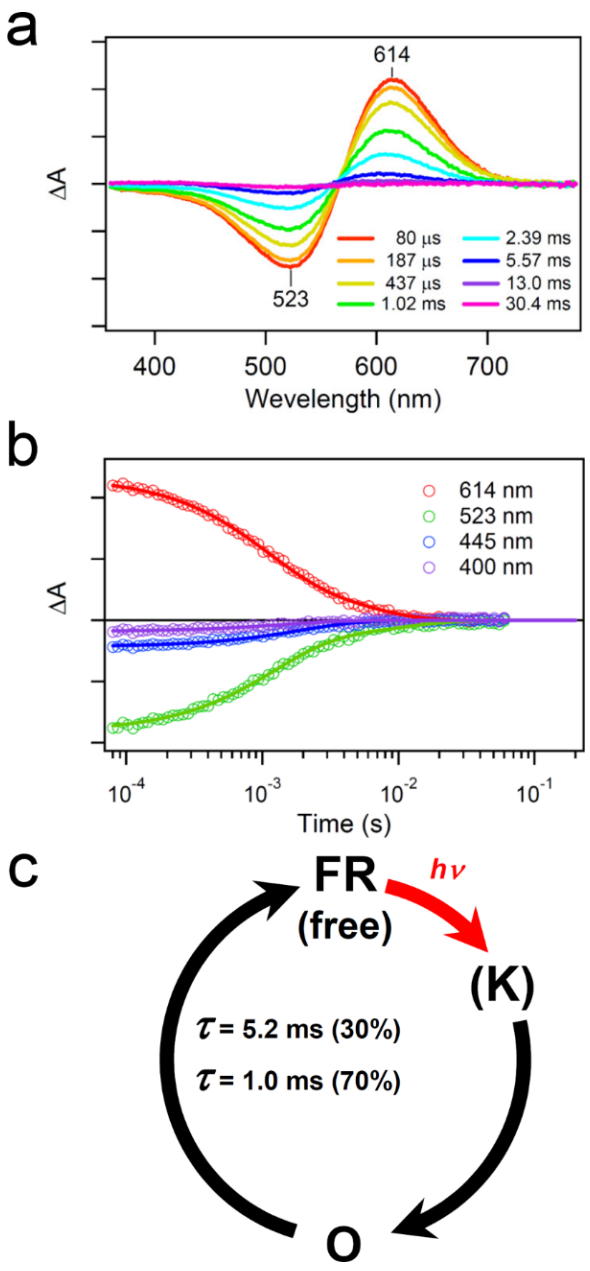

Figure 5-5 Photocycle with no pumping function of FR (no salt).

(a) Transient absorption spectra of FR. (b) Time-evolution at specific wavelengths. (c) Photocycle scheme of FR in the absence of NaCl.

5-4 Discussion

FR is evolutionarily very distant from HR, a well-studied chloride-ion pump, as shown in Figure 1b. In fact, the amino acid sequence of FR is closer to the sodium-ion pump KR2 (33 % identity) than the chloride-ion pumps in haloarchaea (25 % similarity with *s*HR and 23 % similarity with *p*HR). However, the present study revealed a similarity in the molecular properties between FR and HR. Unlike the sodium-ion binding site of KR2, a chloride ion binds near the retinal chromophore in FR as well as in HR. Chloride-ion binding causes a spectral blue shift (Figure 5-2), presumably because of the localization of the positive charge in the Schiff base region. A primary reaction forms the red-shifted K intermediate, which decays to the L intermediate in several μs (Figure 5-3). The Schiff base is not deprotonated during the photocycle, i.e., there is no formation of the M intermediate. The L intermediate is the key state of the vectorial pump because it does not appear during the photocycle of the chloride ion-free form (Figure 5-5). The O intermediate appears at the end of the photocycle. These properties are common between FR and HR, and the light-driven chloride-ion pump functions by a common mechanism.[22]

On the other hand, there are several differences between FR and HR. Binding affinity of the chloride ion is lower in FR (K_d = 84.0 mM) than in HR (K_d = 3 mM for *p*HR),[22] although such a high K_d value is not problematic under the Cl^- concentration of the ocean (~560 mM). While the uptake of a chloride ion occurs upon decay of the O intermediate in HR, it only takes place upon when the O intermediate increases in FR, indicating that FR possesses a transient chloride-ion binding site at the extracellular domain. Below we discuss further details of the similarities and differences between FR and HR, two evolutionarily distinct chloride-ion pumps.

Protein structure and chloride-ion binding site in FR and HR.

Figure 5-6a shows 10 amino acids that differ between *p*HR and FR among 23 amino acid residues within 5 Å from the retinal chromophore in *p*HR.[22] These differences can be summarized as two residues in helix B (S77 and A78 in FR), four in helix C (A126, S130, V131, L134), two in helix E (G180, T184), one in helix F (Y229), and one in helix G (T255). Note that different amino acids are distributed on both sides of the chromophore; seven at the Schiff base and three on β-ionone ring sides. On the other hand, amino acids along the polyene chain are highly conserved. Therefore, different molecular properties of FR originate from these amino acids near the retinal chromophore. In fact, the amino acid at position 255 in *p*HR is known to affect the color of microbial rhodopsin, where the O-H-bearing group shows a spectral blue shift.[23, 24] It is likely that the replacement of A by T in FR contributes to the blue-shifted absorption of FR (λ_{max}: 518 nm) compared to HR (λ_{max}: 576 nm).

Most microbial rhodopsins contain an electric quadrupolar structure with two positive and negative charges in the Schiff base region.[22] For instance, in the Schiff base region of BR, two positive charges are located at the protonated Schiff base and at R82, and counterbalance negative charges located at D85 and D212. The quadrupole inside the protein is stabilized by three water molecules in BR. A complex Schiff base counterion in the electric quadrupole results in weakening of the electrostatic interaction between the Schiff base and the counterion, leading to the spectral red-shift.[23, 24] In *p*HR, the negative charge of D85 is replaced by a chloride ion near the corresponding amino acid threonine, where the protonated Schiff base, R123, chloride ion, and D252 constitute the quadrupole, which is also stabilized by three water molecules (Figure 5-6b). Similar molecular properties with evolutionarily distant proteins suggest the important role of the electric quadrupole while other structural components could be flexible.

In *p*HR, the chloride-ion binding site is comprised of V77, S78, S81, R123, T126, W127, S130, T131, D252, and K256, which contains five O-H-bearing groups (S or T) (Figure 5-6b). FR contains three O-H-bearing groups (S or T) in the corresponding amino acids. Fewer amino acids with an O-H group may be the reason for the weaker affinity of chloride-ion binding in FR. While the chloride ion is not the direct hydrogen-bonding acceptor of the protonated Schiff base in *s*HR and *p*HR,[23-25] halide-dependent color changes in Table 5-1 suggest the direct hydrogen-bonding interaction of the protonated Schiff base with a chloride ion in FR. Detailed analysis of the hydrogen-bonding network in the Schiff base region is intriguing, and our future focus.

Photocycle dynamics and molecular mechanism of chloride pump in FR and HR.

The present flash photolysis study revealed similar photocycle dynamics between FR and HR. The primary reaction of FR is probably the all-*trans* to 13-*cis* photoisomerization in an ultrafast timescale, which forms the primary K intermediate that decays to subsequent intermediates in an early μs regime. Formation of the L intermediate suggests a strong interaction of the retinal chromophore with a chloride ion in FR, as well as in HR. In the case of HR, the two L states, denoted by L_1 and L_2 (or L and N) intermediates, are strongly coupled to the ejection of a chloride ion into the cytoplasmic side.[25,31] Similar multiple L states also likely exist for the FR photocycle. In the absence of a chloride ion, the L intermediate does not appear (Figures 5-5 and S5-4), and no chloride-ion pump exists. The chloride-ion binding site of FR is stabilized by a hydrogen-bonding network, and a hydroben-bonding alteration initited by retinal isomerization makes the vectorial transport of the chloride ion into the cytoplasmic side. The L intermediate is strongly coupled to the process in both FR and HR. In HR, the L intermediate (λ_{max}: 520-530 nm) is clearly blue-shifted from the

unphotolyzed state (λ_{max}~580 nm), and the blue-shifted absorption is one of the characteristics of the L intermediate. In contrast, the L intermediate of FR exhibits λ_{max} at 520-530 nm (Figure 5-3c), which is rather red-shifted from the unphotolyzed state (λ_{max}: 518 nm) (Figure 5-2a). Interstingly, both L states show a similar λ_{max} between FR and HR, although the λ_{max} of the unphotolyzed states differs by >60 nm. This may suggest that the specific interaction between the chromophore and chloride ion is more predominant for color tuning in the L intermediate than in the surrounding amino acids.

At the end of the photocycle, the O intermediate appears. In the case of HR, chloride-ion uptake occurs upon the decay of O, suggesting that the chloride ion is directly transported from aqueous solution to its binding site near the Schiff base. On the other hand, chloride-ion uptake of FR occurs upon the formation of O. This suggests the transient formation of a chloride-ion binding site near the extracellular surface in the O intermediate. This difference in the O intermediate of FR and HR is intriguing from a mechanistic point of view. A light-driven chloride-ion pump must have an alternative access mechanism, where accessibility changes transiently between the extracellular and cytoplasmic sides.[10] In the unphotolyzed state of FR and HR, the cytoplasmic side is closed, the extracellular side is open and a chloride-ion binding equilibrium occurs on the extracellular side.[23,24] During the photocycle, the cytoplasmic side opens, by which chloride-ion release is possible. Such a change in access must occur with the decay of the L (L_2) intermediate. An important aspect is that at that time, the opposite extracellular side should be occluded. Otherwise, back-flow of chloride ion toward the extracellular side may take place. A difference in timing of chloride-ion uptake between FR and HR suggests different accessibility of the O intermediate, where the cytoplasmic side is occluded after the release of the chloride ion. The O intermediate of HR possesses an occluded structure for both extracellular and cytoplasmic sides, so that

chloride-ion uptake occurs upon the decay of O. In contrast, it is likely that the O intermediate of FR possesses an open structure on the extracellular side, so that a chloride ion is taken up to the second binding site. Note that the uptake of a sodium ion occurs from the cytoplasmic aqueous phase exclusively upon the rise of O, but not its decay, for the light-driven sodium-ion pump KR2.[12] In contrast, in FR, the uptake of a chloride ion occurs from the extracellular aqueous phase not only upon the rise of O, but also upon its decay (Figure 5-4). This suggests that the second binding site of the chloride ion is not tightly coupled to the Schiff base region.

At this moment, there is no information about the second binding site of the chloride ion. It may be only created for the photocycle intermediate. Alternatively, the chloride ion is able to bind the second site, even in the unphotolyzed state. While these details will be studied in the future, the sodium binding site in KR2 should be noted. We recently reported the presence of a light-driven sodium-ion pump (KR2) from a marine bacterium which contains the binding site of sodium ion near the extracellular surface.[12] In fact, four carboxylates in the B-C loop are responsible for sodium-ion binding. Binding is not a prerequisite for the sodium-ion pump, but sodium-ion binding at the extracellular surface must play a physiological role such as protein stability.[12] Localization of a second binding site in FR, NTQ rhodopsin, and its relation to the sodium-ion binding site in KR2, are also interesting.

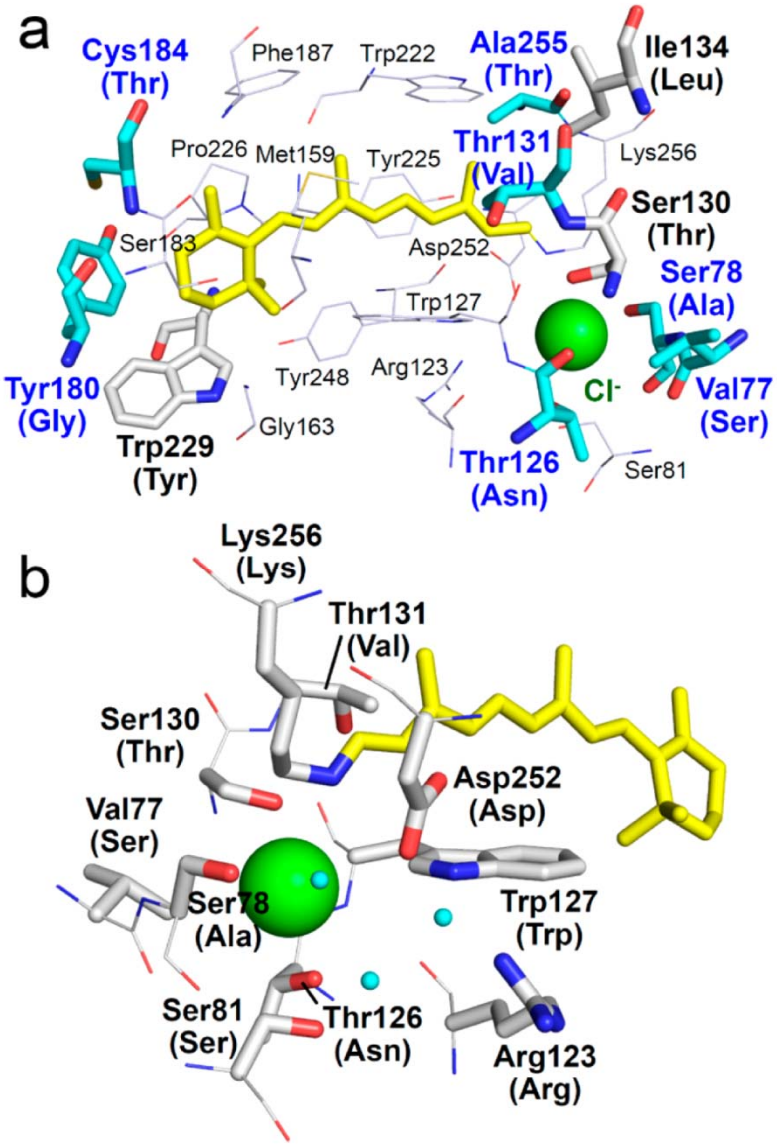

Figure 5-6. Amino acid comparison between *Np*HR and FR

(a) X-ray crystallographic structures of *Np*HR (PDB entry: 3A7K).[23] Among 23 amino acid residues within 5 Å from the retinal chromophore, 10 are different between *Np*HR (written with a number) and FR (written in parentheses), which are further classified into conserved (black) or different (blue) amino acids. (b) Enlarged chloride binding site. Protein-bound water molecules are shown by a blue ball.

5-5 Conclusion

Using spectroscopic methods, we studied the molecular properties of a eubacterial light-driven chloride-ion pump, FR. The obtained molecular mechanisms for FR are essentially common for HR, although FR and HR are evolutionarily distinct. This common mechanism suggests the importance of the electric quadrupole in the Schiff base region and their changes through hydrogen-bonding alterations. On the other hand, other regions are more flexible, and it seems that common structural changes in microbial rhodopsins are sufficient. Finding new chloride-ion pumps such as FR with a common mechanism with HR opens up various possibilities in basic and applied research fields. As a basic science, the detailed molecular mechanisms of light-driven chloride-ion pumps will be further examined. An interesting aspect is the functional conversion by mutation. In the case of haloarchaeal proton (BR) and chloride-ion (HR) pumps, the former can be converted into the latter by a single amino acid replacement (D85T BR).[25] However, HR cannot be converted into a proton pump even by multiple mutations, and this asymmetric functional conversion has been interpreted by a water-containing hydrogen-bonding network in the Schiff base region.[258] It is intriguing whether such a mechanism is true for light-driven proton and chloride-ion pumps from marine bacteria, to which a sodium-ion pump can be additionally tested. In applied research, FR may be a potential tool in optogenetics where HR has been used as a neural silencer.[26] Although the intact binding affinity of the chloride ion is not high, molecular designs can be tested for optogenetic applications.

REFERENCES

(1) Ernst, O. P.; Lodowski, D. T.; Elstner, M.; Hegemann, P.; Brown, L. S.; Kandori, H. Microbial and animal rhodopsins: structures, functions, and molecular mechanisms. Chem. Rev. 2014, 114, 126-63.

(2) Oesterhelt, D.; Stoeckenius, W. Rhodopsin-like protein from the purple membrane of Halobacterium halobium. Nat. New Biol. 1971, 233, 149-52.

(3) Matsuno-Yagi, A.; Mukohata, Y. Two possible roles of bacteriorhodopsin; a comparative study of strains of Halobacterium halobium differing in pigmentation. Biochem. Biophys. Res. Commun. 1977, 78, 237-43.

(4) Schobert, B.; Lanyi, J. K. Halorhodopsin is a light-driven chloride pump. J. Biol. Chem. 1982, 257, 10306-13.

(5) Béjà, O.; Aravind, L.; Koonin, E. V.; Suzuki, M. T.; Hadd, A.; Nguyen, L. P.; Jovanovich, S. B.; Gates, C. M.; Feldman, R. A.; Spudich, J. L.; Spudich, E. N.; DeLong, E. F. Bacterial rhodopsin: evidence for a new type of phototrophy in the sea. Science 2000, 289, 1902-6.

(6) Sharma, A. K.; Spudich, J. L.; Doolittle, W. F. Microbial rhodopsins: functional versatility and genetic mobility. Trends Microbiol. 2006, 14, 463-9.

(7) DeLong, E. F.; Beja, O. The light-driven proton pump proteorhodopsin enhances bacterial survival during tough times. PLoS Biol. 2010, 8, e1000359.

(8) Bamann, C.; Bamberg, E.; Wachtveitl, J.; Glaubitz, C. Proteorhodopsin. Biochim. Biophys. Acta 2014, 1837, 614-25.

(9) Váró, G. Analogies between halorhodopsin and bacteriorhodopsin. Biochim. Biophys. Acta 2000, 1460, 220-9.

(10) Essen, L. O. Halorhodopsin: light-driven ion pumping made simple? Curr. Opin. Struct.

Biol. 2002, 12, 516-22.

(11) Miranda, M. R.; Choi, A. R.; Shi, L.; Bezerra, A. G., Jr.; Jung, K. H.; Brown, L. S. The photocycle and proton translocation pathway in a cyanobacterial ion-pumping rhodopsin. Biophys. J. 2009, 96, 1471-81.

(12) Inoue, K.; Ono, H.; Abe-Yoshizumi, R.; Yoshizawa, S.; Ito, H.; Kogure, K.; Kandori, H. A light-driven sodium ion pump in marine bacteria. Nat. Commun. 2013, 4, 1678.

(13) Brown, L. S. Eubacterial rhodopsins - unique photosensors and diverse ion pumps. Biochim. Biophys. Acta. 2014, 1837, 553-61.

(14) Yoshizawa, S.; Kumagai, Y.; Kim, H.; Ogura, Y.; Hayashi, T.; Iwasaki, W.; DeLong, E. F.; Kogure, K. Functional characterization of flavobacteria rhodopsins reveals a unique class of light-driven chloride pump in bacteria. Proc. Natl. Acad. Sci. USA 2014, 111, 6732-7.

(15) Luecke, H.; Schobert, B.; Stagno, J.; Imasheva, E. S.; Wang, J. M.; Balashov, S. P.; Lanyi, J. K. Crystallographic structure of xanthorhodopsin, the light-driven proton pump with a dual chromophore. Proc. Natl. Acad. Sci. USA 2008, 105, 16561-5.

(16) Ono, H.; Inoue, K.; Abe-Yoshizumi, R.; Kandori, H. FTIR spectroscopy of a light-driven compatible sodium ion-proton pumping rhodopsin at 77 K. J. Phys. Chem. B 2014, 118, 4784-92.

(17) Jones, D. T.; Taylor, W. R.; Thornton, J. M. The rapid generation of mutation data matrices from protein sequences. Comput. Appl. Biosci. 1992, 8, 275-82.

(18) Tamura, K.; Peterson, D.; Peterson, N.; Stecher, G.; Nei, M.; Kumar, S. MEGA5: molecular evolutionary genetics analysis using maximum likelihood, evolutionary distance, and maximum parsimony methods. Mol. Biol. Evol. 2011, 28, 2731-9.

(19) Váró, G.; Needleman, R.; Lanyi, J. K. Light-driven chloride ion transport by

halorhodopsin from Natronobacterium pharaonis. 2. Chloride release and uptake, protein conformation change, and thermodynamics. Biochemistry 1995, 34, 14500-7.

(20) Kolbe, M.; Besir, H.; Essen, L. O.; Oesterhelt, D. Structure of the light-driven chloride pump halorhodopsin at 1.8 A resolution. Science 2000, 288, 1390-6.

(21) Shibata, M.; Muneda, N.; Sasaki, T.; Shimono, K.; Kamo, N.; Demura, M.; Kandori, H. Hydrogen-bonding alterations of the protonated Schiff base and water molecule in the chloride pump of Natronobacterium pharaonis. Biochemistry 2005, 44, 12279-86.

(22) Kouyama, T.; Kanada, S.; Takeguchi, Y.; Narusawa, A.; Murakami, M.; Ihara, K. Crystal Structure of the Light-Driven Chloride Pump Halorhodopsin from Natronomonas pharaonis. J. Mol. Biol. 2010, 396, 564-579.

(23) Sudo, Y.; Yuasa, Y.; Shibata, J.; Suzuki, D.; Homma, M. Spectral tuning in sensory rhodopsin I from Salinibacter ruber. J. Biol. Chem. 2011, 286, 11328-36.

(24) Inoue, K.; Tsukamoto, T.; Sudo, Y. Molecular and evolutionary aspects of microbial sensory rhodopsins. Biochim. Biophys. Acta 2013, 1837, 562-77.

(25) Sasaki, J.; Brown, L. S.; Chon, Y. S.; Kandori, H.; Maeda, A.; Needleman, R.; Lanyi, J. K. Conversion of bacteriorhodopsin into a chloride ion pump. Science 1995, 269, 73-5.

(26) Chow, B. Y.; Han, X.; Dobry, A. S.; Qian, X.; Chuong, A. S.; Li, M.; Henninger, M. A.; Belfort, G. M.; Lin, Y.; Monahan, P. E.; Boyden, E. S. High-performance genetically targetable optical neural silencing by light-driven proton pumps. Nature 2010, 463, 98-102.

Supporting Information

Methodology of the analysis of transient absorption change.

The transient absorption change of FR obtained by the flash-photolysis experiment was analyzed according to the methodology reported by Klinger and Braiman.[1] The absorption spectra at different time-points are expressed by a n×m matrix (**A**(*n*, *m*)) where n and m are the number of wavelengths and time-points (80 μs - 150 ms) of the data, respectively. Singular value decomposition (SVD) represents **A** by three matrixes (**U**, **S**, and **V**) as $\mathbf{A} = \mathbf{USV}^T$. **U** and **V** each consist of columns of orthonormal vectors. The columns of **U** are called the basis spectra. On the other hand, the column elements of **V** represent time courses. **S** is a diagonal matrix and the *n* elements are called singular values of **A**. The magnitude of the *n*th singular value represents the degrees of contribution of the *n*th column component of **U** and **V** to **A**. The diagonal elements of **S** (singular values) are arranged in the order of decreasing values. The highest singular value corresponding to the first columns of **U** and **V** most strongly contribute to **A**. In contrast, the lower values contain only information about noise. In the current case, we found that while only two components with the largest singular values showed a meaningful absorption change and time-course (Fig. S4a and S4b), the other components with smaller singular values contained only the noisy feature. Thus, we concluded that it is sufficient to express the transient absorption change of FR with two basis spectra (U1 and U2) and two time courses (V1 and V2) with the largest singular values.

V1 and V2 were analyzed by a multi-exponential function. As a result, they could by expressed by the sum of four-exponential functions whose lifetimes are τ = 250 μs, 2.6 ms, 3.7 ms and 20.4 ms, respectively. This result indicates that four elementary processes of the reaction are present in the photocycle of FR at t ≥ 80 μs. The time-evolution of the

absorption change at each wavelength of **A** can be analyzed by global fitting with four exponentials with these lifetimes. Consequently, **A** can be expressed as follows:

$$\mathbf{A} = \begin{bmatrix} DAS_1 \end{bmatrix} \begin{bmatrix} \exp(-t/\tau_1) \\ \exp(-t/\tau_2) \\ \exp(-t/\tau_3) \\ \exp(-t/\tau_4) \end{bmatrix} \quad \text{Eq. S1.}$$

where, DAS_i is the decay-associated-spectrum which represents the amplitude of *i*-th components with a lifetime of τ_i ($\tau_1 < \tau_2 < \tau_3 < \tau_4$). DAS_i contains information about spectral change along the period of accumulation of photo-intermediates, as follows:

$$\begin{bmatrix} DAS_1(\lambda) \\ DAS_2(\lambda) \\ DAS_3(\lambda) \\ DAS_4(\lambda) \end{bmatrix} = \begin{bmatrix} 1 & \frac{k_1}{k_2-k_1} & \frac{k_1k_2}{(k_2-k_1)(k_3-k_1)} & \frac{k_1k_2k_3}{(k_2-k_1)(k_3-k_1)(k_4-k_1)} \\ 0 & \frac{k_1}{k_1-k_2} & \frac{k_1k_2}{(k_1-k_2)(k_3-k_2)} & \frac{k_1k_2k_3}{(k_1-k_2)(k_3-k_2)(k_4-k_2)} \\ 0 & 0 & \frac{k_1k_2}{(k_1-k_3)(k_2-k_3)} & \frac{k_1k_2k_3}{(k_1-k_3)(k_2-k_3)(k_4-k_3)} \\ 0 & 0 & 0 & \frac{k_1k_2k_3}{(k_1-k_4)(k_2-k_4)(k_3-k_4)} \end{bmatrix} \begin{bmatrix} \Delta A_1(\lambda) \\ \Delta A_2(\lambda) \\ \Delta A_3(\lambda) \\ \Delta A_4(\lambda) \end{bmatrix} \quad \text{Eq. S2}$$

where k_i and ΔA_i are the rate constant and difference spectra between the i-th component and the initial state. Thus, we can calculate ΔA_1-ΔA_4 from Eq. S2 (Fig. S4d).

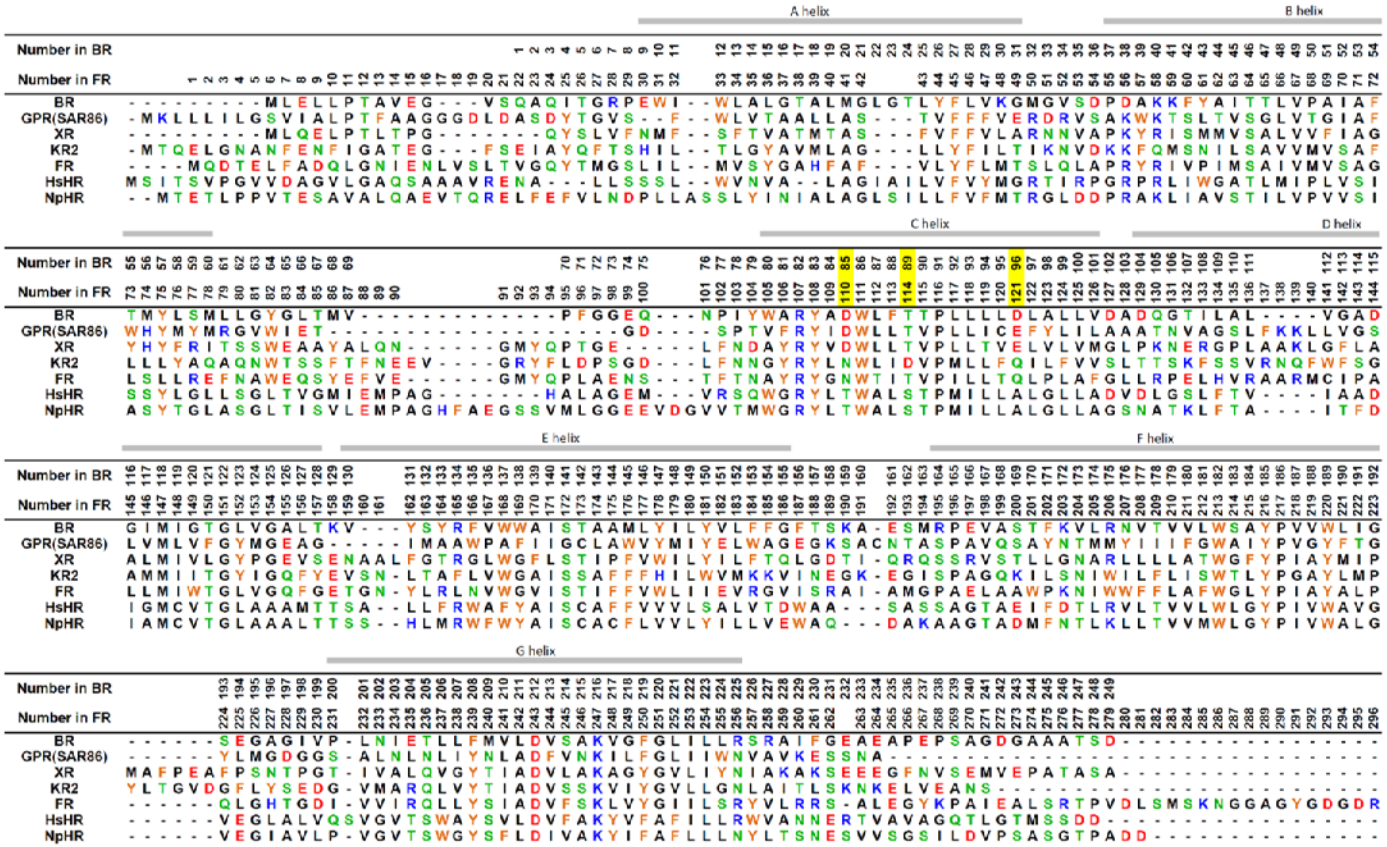

Figure S5-1. Amino-acid sequences of microbial rhodopsins, BR: bacteriorhodopsin, GPR (SAR86): Green proteorhodopsin, XR: Xanthorhodopsin, KR2: *Krokinobacter* rhodopsin 2, FR: *Fulvimarina* rhodopsin, HsHR: Halorhodopsin from *Halobacterium salinarum*, NpHR: Halorhodopsin from *Natronomonas pharaonis*.

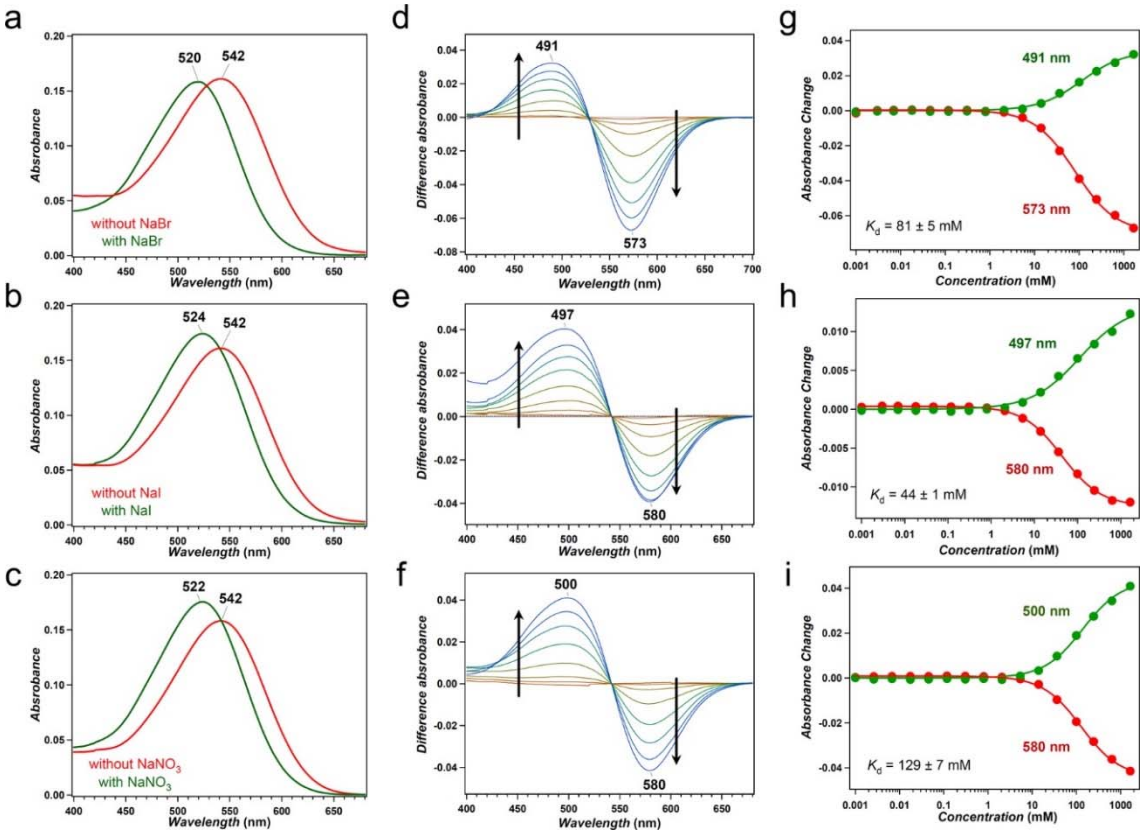

Figure S5-2. Absorption spectral changes of FR in response to different salt concentrations. Absorption spectra of FR in solvent containing 0 mM (green) and 1660 mM (a) NaBr (red), (b) NaI (red) and (c) $NaNO_3$. Absorption spectral changes of FR upon addition of (d) NaBr, (e) NaI and (f) $NaNO_3$ (2.1, 5.4, 14, 36, 100, 250, 640, 1660 mM vs 0 mM). Arrows indicate the direction of change with increasing salt concentration. (g-i) Absorption changes at wavelengths of negative and positive peaks in (d-f) for the concentration change of (g) NaBr, (h) NaI and (i) $NaNO_3$. Solid lines indicate fitting curves using the Hill equation with n=1.

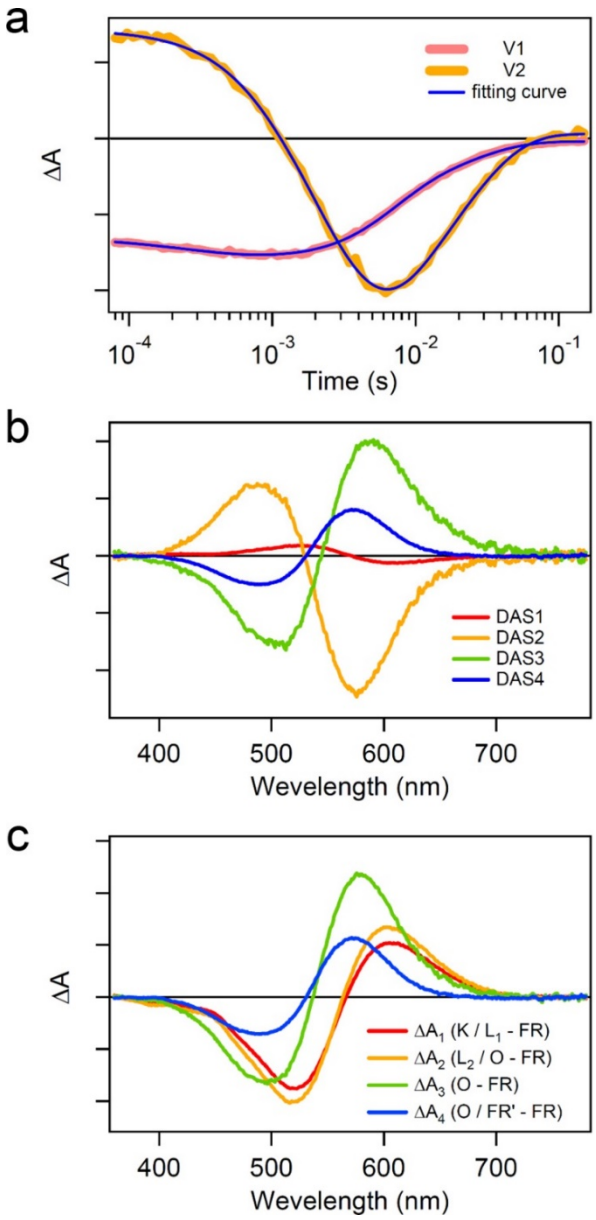

Figure S5-3. Basis spectra (a) and time courses (b) corresponding to the two largest singular values. (c) Decay associated spectra (DAS) of transient absorption change of photo-excited FR. DAS1, DAS2, DAS3 and DAS4 represent the amplitudes of absorption change of four exponentially decaying components with lifetimes of 250 μs, 2.6 ms, 3.7 ms and 20.4 ms, respectively. (d) Difference absorption spectra between four intermediate states and the initial state of FR calculated from DASs shown in Fig. S4b.

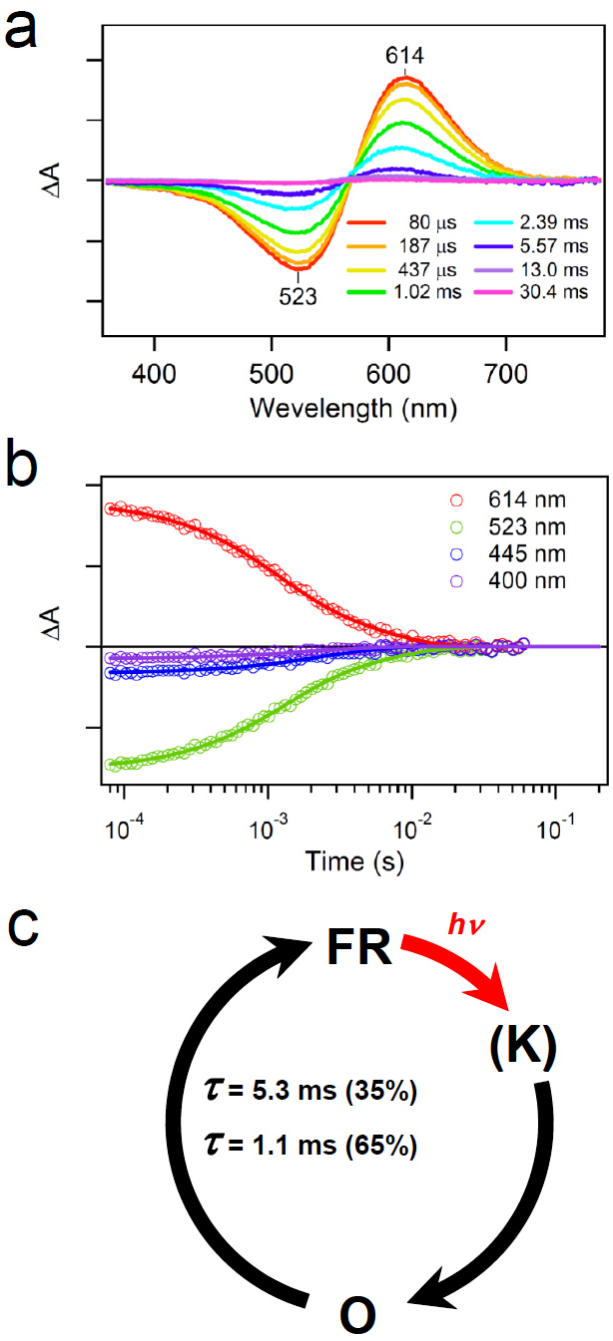

Figure S5-4. Photocycle of FR in a solution containing 33 mM Na_2SO_4. (a) Transient absorption spectra of FR. (b) Time-evolution at specific wavelengths. (c) Photocycle scheme of FR in a solution containing 33 mM Na_2SO_4

References

(1) Klinger, A. L.; Braiman, M. S. Structural comparison of metarhodopsin II, metarhodopsin III, and opsin based on kinetic analysis of Fourier transform infrared difference spectra. *Biophys. J.* **1992,** *63*, 1244-55.

Chapter 6

Conclusion & Perspectives

6-1 Conclusion

In chapter 1, background and purpose of my studies are explained. Recent genomic analysis and optogenetics encourage rhodopsin field. We focused on newly identified NDQ and NTQ rhodopsins which have light-driven sodium pump and chloride pump, respectively.

In chapter 2, Functional study based on the crystallographic structures were shown. We proposed that the rotation of D116, proton acceptor of Schiff base allow Na^+ influx near Schiff base. Furthermore, we achieved to create light-driven potassium pump by introducing two mutation based on structure.

In chapter 3, H^+-Na^+ selectivity during ion uptake transition of KR2 was estimated by kinetic analysis. The selectivity value (k_H/k_{Na}) is $>10^3$, indicating that H^+ uptake occurs dominantly if [Na^+] is comparable to [H^+]. But, the value allows KR2 take up Na^+ in physiological condition.

In chapter 4, The creation of Engineered KR2 which can transport Cs+ was shown. Two amino acids constructing intracellular cavity were related cation selectivity.

In chapter 5, light-driven chloride pump which has NTQ motif, FR was studied. Although the amino acid sequence identity between FR and well-studied chloride pump HR is low, FR has similar properties with HR.

Although the main purpose of these studies is to reveal the functional mechanism of ion-transport rhodopsins, the perceptions obtained from these studies are applicable to other fields such as neuroscience, environmental and energy field. “Light-driven” function is very useful. And, microbial rhodopsins have variable in its functions and absorption spectra. In addition, thermostability of microbial rhodopsin is relatively higher than other proteins. Thus, it is expected that studies of microbial rhodopsin will be continued and be widely extended.

Acknowledgements

I would like to thank Professor Hideki Kandori from Nagoya Institute of Technology, who supervised my work. I am deeply indebted to him for the thinking of science and my life.

I would like to thank Dr. Keiichi Inoue from Nagoya Institute of Technology, who taught me experimental techniques and discuss about my work.

I am grateful to all collaborators and also like to thank Kandori laboratory's members who helped my experiment and discussed my work.

Finally, I would especially like to thank my parents: Kenji Kato and Terumi Kato. Special thanks for supporting my mental in the Ph. D course.

2015, January, Yoshitaka Kato